POLITECNICO
MILANO 1863

SCUOLA DI INGEGNERIA INDUSTRIALE
E DELL'INFORMAZIONE

Strut-Braced Wing Aircraft Configuration: An Aeroelastic Assessment

Tesi di Laurea Magistrale in
Aeronautical Engineering - Ingegneria Aeronautica

Author: **Elena Roncolini**

Student ID: 926895
Advisor: Prof. Sergio Ricci
Co-advisors: PhD Francesco Toffol
Academic Year: 2022-23

*Ogni psada in dal c*l l'at para avanti n'pas.*

Abstract

Climate change is a serious problem. In the last century, globalization have brought to an extended employment of carbon-based fuels, which can be identified as the main reason for atmospheric pollution. All the transport sector is involved, with no exception for aviation. A massive intervention is required. In European Union (EU) several initiatives have been proposed to this aim, one of which is called Clean Sky 2. In this context, a project named U-HARWARD has been funded to investigate the use of innovative aerodynamic and aeroelastic designs by means of a multi-fidelity multi-disciplinary optimal approach. One of the tasks was to study a promising unconventional configuration: the Strut-Braced Wing (SBW). The idea behind this concept is to increase as much as possible the aerodynamic efficiency, by decreasing the induced drag. A (ultra-)high wing Aspect Ratio (AR) is used. However, this alone causes a significant increase in wing bending moment and, consequently, in wing weight. To keep limited weight, a strut can be exploited, whose function is to alleviate wing bending moment by preventing too high deformations. An overconstrained system, which is intrinsically complex, is obtained. Due to the unconventional nature of this configuration, along with high flexibility of such increased AR, unexpected aeroelastic behaviors could occur. After having created a suitable SBW model, the present thesis focuses on classical aeroelastic studies such as trim, gust response, divergence and flutter. When allowed, both linear and nonlinear analyses have been computed, highlighting the importance of considering nonlinearity when large displacements can be reached, as in this case. Finally, some parametric analyses have been investigated, to check which is the influence of wing and strut material, mass configuration, strut geometry and wing-strut attachment chordwise position on the results. SBW seems a promising configuration, allowing for very high ARs still reducing the weight with respect to Classical Tube and Wing (CTW) aricrafts. However, some attention must be posed on strut design: if it is too flexible, it looses its benefits, causing some unexpected deformations. To reduce the weight increment associated to a larger strut, composites can be employed, leading to a lighter yet stiff structure.

Keywords: Strut-Braced Wing (SBW), nonlinear aeroelasticity

Sommario

Il cambiamento climatico è un serio problema. Nell'ultimo secolo, la globalizzazione ha causato un ampio impiego di combustibili fossili, i quali possono essere identificati come la principale causa dell'inquinamento atmosferico. Tutto il settore dei trasporti è coinvolto, senza eccezione per l'aviazione. Un intervento massiccio è necessario. Nell'Unione Europea sono state proposte varie iniziative a questo scopo, una delle quali si chiama Clean Sky 2. In questo contesto, è stato finanziato un progetto chiamato U-HARWARD, il cui scopo è quello di studiare l'uso di design innovativi per l'aerodinamica e l'aeroelasticità, ricorrendo a un approccio multi-fedeltà multi-disciplinare di ottimo. Uno degli obiettivi del progetto era quello di studiare una configurazione non convenzionale apparsa promettente: lo Strut-Braced Wing (SBW). L'idea dietro a tale concetto è quella di aumentare il più possibile l'efficienza aerodinamica diminuendo la resistenza indotta. Per fare ciò, è stato introdotto un (ultra-)elevato allungamento alare, che tuttavia produrrebbe un aumento significativo del momento flettente per l'ala e di conseguenza del suo peso. Per ovviare questo problema, si è pensato di ricorrere a uno strut (montante o controvento), il quale ha lo scopo di alleviare i carichi nell'ala, trattenendola e limitandone le deformazioni. Si ha in questo modo un sistema iperstatico, il quale è intrinsecamente complicato. La natura non convenzionale di tale configurazione, congiuntamente all'alta flessibilità dovuta all'elevato allungamento alare, potrebbe avere degli effetti inaspettati sull'aeroelasticità del velivolo. Dopo aver creato un modello di SBW, la presente tesi si focalizza sulle classiche analisi aeroelastiche: trim, risposta a raffica, divergenza e flutter. Dove possibile, sono state svolte sia analisi lineari che nonlineari, perché strutture molto flessibili, come in questo caso, possono raggiungere grandi spostamenti. Infine, sono state svolte alcune analisi parametriche cambiando il materiale di ala e strut, la configurazione di massa, la geometria dello strut e la posizione in corda dell'attacco tra ala e strut. Lo SBW sembra effettivamente promettente, permettendo elevati allungamenti alari mantenendo comunque un peso ridotto rispetto alle configurazioni convenzionali. Tuttavia, bisogna fare attenzione al design dello strut: se troppo flessibile, lo strut non lavora correttamente, causando deformazioni inaspettate. D'altro canto, aumentarne le dimensioni significa aumentarne il peso. Ciò non rappresenta di per sé un problema. Infatti, utiliz-

zando materiali compositi, si è visto che si ottiene una diminuzione significativa di peso pur mantenendo una rigidezza adeguata.

Parole chiave: Strut-Braced Wing (SBW), aeroelasticità nonlineare

Contents

Introduction

Climate changes should happen because of nature. Unfortunately, starting from the last century, human activities have become the main reason for these phenomena to occur. In particular, carbon-based fuels released CO_2 is one of the principal concerns. Since these fuels are employed practically in every sector (e.g. industry, agriculture, energy, transport), it's easy to understand the need for everyone to actively participate in the attempt to reduce the emissions. Of course, also the aviation world is involved. Indeed, as reported by the International Energy Agency in [1], in 2021 air transports were responsible for over 2% of global CO_2 emissions.

In this context, a EU funded Clean Sky 2 project leaded by POLIMI was started in May 2020, as a response to the call JTI-CS2-2019-CFP10-THT-07, whose name is U-HARWARD, acronym of Ultra-High Aspect Ratio Wing Advanced Research and Designs [2]. The aim of the project is to investigate the use of innovative aerodynamic and aeroelastic designs exploiting a multi-fidelity multi-disciplinary optimal design approach in order to develop (Ultra-)High Aspect Ratio Wings ((U)HARW) for medium and large transport aircrafts.

Before proceeding, it could be useful to try to understand why the interest has been posed on HARW. A recall to the Breguet range formula (1), whose terms are reported in List of Symbols, can be needed at this point.

$$R = \frac{V_{TAS}}{g}\left(\frac{L}{D}\right)\frac{1}{SFC}ln\left(\frac{W_{MTOW}}{W_{MTOW} - W_{fuel}}\right) \tag{1}$$

This equation shows how the aircraft efficiency is impacted by: aeordynamics, by means of L-to-D ratio, propulsion, by means of Specific Fuel Consumption (SFC) and structure, by means of logaritmic term. When an aerodynamicist looks at (1), focuses on L-to-D ratio, where L is the lift and D is the drag. In particular, D can be subdivided in several contributions, e.g. wave drag, induced drag, friction drag. Acting on specific geometric parameters of the aircraft allows to directly act on these components. Specifically, induced drag, which is the most relevant one, can be decreased by increasing the wing AR. Consequently, HARWs present higher L-to-D ratios, which translates in smaller fuel

consumptions and smaller emissions. The problem arises with the structurist. Indeed, higher ARs mean higher wing weight, which requires more fuel. It's a matter of trade-offs, which is the reason why treating the problem through a multi-disciplinary approach is desirable.

The consortium working on U-HARWARD is composed by Politecnico di Milano, i.e. the coordinator, IBK Innovation GmbH & Co. KG, University of Bristol, Office National d'Etudes et de Recherches Aérospatiales (ONERA), Institut Supérieur de l'Aéronautique et de l'Espace (ISAE-SUPAERO) and Siemens Industry Software SAS. U-HARWARD research can be split in three main activities: the first is to understand for which wing AR a minimum fuel consumption is reached for a Classical Tube and Wing (CTW) configuration. Since an increase in AR is expected to be beneficial for lowering the emissions, the second acitivity is to study an unconventional configuration that appeared to be promising, that is the Strut-Braced Wing (SBW). As explained before, increasing the AR generates an increase in wing weight, since the wing bending moment increases and more material is required to sustain it. In order to reduce this weight penalty, a strut can be used to limit the deflection of the wing, which translates in an alleviation of wing bending moment, allowing margins for weight reduction even with high ARs. Of course, this unconventional configuration has some issues that must be adressed: which are the most effective chord- and span-wise positions for the strut? How much must the strut be flexible? Is the strut a lifting surface? Where must the engines be located? And several other questions. The third and last activity regards a new technology related to both airport capacity and load alleviation, which is the Folding Wing Tip (FWT). Indeed, having high AR could cause logistic problems at the airport gates, which can be solved folding the outer portions of the wing exploiting a hinge-like mechanism. Moreover, this technology can also be used during flight when a gust is encountered, becoming a load alleviation technology. The interested readers find the last updates of the project in [3].

The present work focuses on SBW unconventional configuration. In particular, after having chosen a baseline aircraft, an aeroelastic model has been produced using NeoCASS [4] [5], an open-source software developed at Politecnico di Milano. When a long and very expensive project, such as the design and manufacturing of an aircraft, is undertaken, it's preferable to know from the beginning all the possible issues, in order to immediately take them into account. Discover, for instance, an adverse aeroelastic behavior during advanced phases of the project is very undesired, because usually it requires to revise some early stages of the design and this could lead to serious changes that are both time and cost consuming. NeoCASS was mainly developed to avoid this occurrence. Indeed, it allows to create a relatively simple model where the structure is composed by a so-called

stick model, while the aerodynamics is inserted through VLM/DLM, at the conceptual design stage. Typical aeroelastic analyses such as trim, flutter, gust response can be computed. It also includes a new optimization module, called NeOPT [6] [7], which acts on the wingbox components structural properties, increasing or reducing them managing possible aeroelastic issues. This workflow is particularly suited for unconventional designs, in which several uncertainties are present. It's even more suited for very flexible aircrafts, where aeroelasticity plays an important role. Being the SBW both unconventional and very flexible due to its high AR, it's very natural to understand the choice of using NeoCASS. To produce the aeroelastic model of the chosen aircraft, a sort of iterative procedure was needed because some issues have been found. Once the final model has been obtained, several aeroelastic analyses have been computed in order to understand its behavior. Then, some changes have been brought and the analyses have been recomputed to understand the impact of some parameters on the design.

Thesis layout

In the first Chapter, a review of working principle and history of SBW is presented.

The second Chapter is entirely dedicated to the model generation. The way the reference model has been chosen is described. Then, some modeling choices are highlighted. The employed tools and followed procedure are explained along with some issues that have been found. A model update has been proposed as solution and some related results are presented. At the end a comparison between CTW and SBW is reported.

The subjects of the third Chapter are aeroelastic analyses. They are briefly described in a theoretical way. Some considerations regarding the importance of nonlinear analyses computations for this unconventional configuration are discussed.

The fourth Chapter focuses on results. The aforementioned analyses are computed and the associated results are shown. In particular, two parts can be distinguished: the first one focuses on the model described in the second Chapter. The last one reports some parametric analyses whose aim is to try to understand how some model changes affect the results. In particular, in the first comparison wing and strut material is changed. In the second one, different mass configurations are considered. In the third one, different strut geometry is accounted for. In the last one, the wing-strut attachment chordwise position is modified.

Finally, a summary of the work, along with conclusions and possible future developments are reported.

1 | State of the art

As already mentioned, air transport is nowadays responsible for a non-negligible portion of CO_2 emissions ($\sim 2\%$). Therefore, bringing flights to a greener level is mandatory. In the last decades, several work has been done to increase aircrafts efficiency. However, it must be admitted that, at this stage, a sort of plateau has been reached. Indeed, for civil aviation the Classical Tube and Wing (CTW) configuration has been globally identified as the winner, and the current most popular models, such as the Airbus A320 family or the Boeing 737 one, with low wing, wing-mounted engines and classical tail, do not differ so much, as seen in Figure 1.1.

(a) A320 [8] (b) B737 [9]

Figure 1.1: Comparison of CTW: A320 vs B737

The next huge change could be represented by the introduction of zero-emission initiatives. However, in order to fully accomplish this task, it's likely that some time still has to pass. Since advanced technolgies, such as alleviation systems, composite materials, advanced aerodynamic profiles allow only for relatively reduced gains, a change of perspective is perhaps needed. For this reason, some interest has been invested in unconventional configurations, where *unconventional* must be intended with respect to CTW. This is the case for Blended Wing Body (BWB), Box-Wing (BW), Strut-Braced Wing (SBW) and Truss-Braced Wing (TBW). An overview of these concepts can be found in [10].

Since this work focuses on the aeroelastic behavior of SBW, in the present Chapter two aspects are treated: the reason why SBW appears appealing for future sustainable aircrafts

and a brief review of its history.

1.1. SBW working principle

In order to reduce aircraft emissions, higher efficiency is required. Aerodynamic efficiency is represented by L-to-D ratio, where L is the lift and D is the drag. Drag can be subdivided into several components. One of the principal is the induced drag, which, as reported in [11], for large transport aircrafts could cover around 43% of the total drag in cruise.

$$C_{D_i} = \frac{C_L^2}{\pi ARe} \tag{1.1}$$

As shown in Equation (1.1), induced drag coefficient depends proportionally on the square of lift coefficient (C_L), and inversely on Oswald coefficient (e) and wing Aspect Ratio (AR). Hence, if AR is increased, the induced drag in decreased. However, increasing the AR means increasing wing bending moment, which leads to increased wing weight, since more bending material must be put in the wing to sustain higher loads. A way to alleviate the wing bending moment keeping high AR for high efficiency is needed. In the presence of a high wing, a strut can be introduced between the lower part of the fuselage and the wing itself. When the wing is loaded with positive lift, it tends to deform a lot due to the high AR and consequent high flexibility, but, thanks to the strut, the deflection along with bending moment remains limited, as qualitatively shown in Figure 1.2.

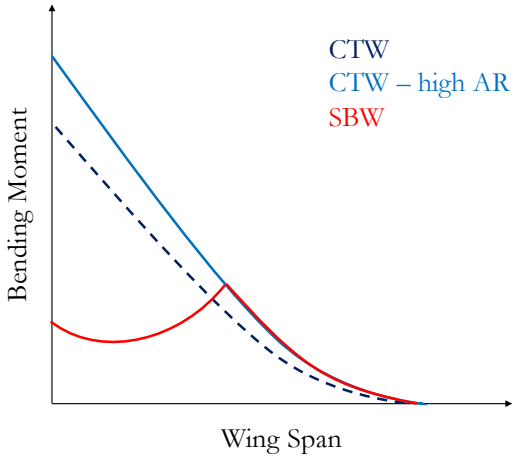

Figure 1.2: Qualitative behavior of wing bending moment for different aircraft configurations

If bending moment is reduced, wingbox thickness can be reduced too, hence thickness-to-chord ratio (t-to-c) is smaller. Since the transonic wave drag depends proportionally on t-to-c, it decreases too. This allows for smaller sweep angles, which, along with the reduced chord caused by the high AR, permit to have smaller Reynolds numbers and consequently an increased area of natural laminar flow. The efficiency gain allows for smaller consumptions, which possibly means smaller engines and smaller noise, as reported for instance in [12]. All these interactions, which include structure, aerodynamics, propulsion, suggest that a multi-disciplinary approach is the best suited for the problem, and it potentially could lead to important gains.

1.2. SBW historical review

Firstly, the distinction between Strut- and Truss-Braced Wing is pointed out.

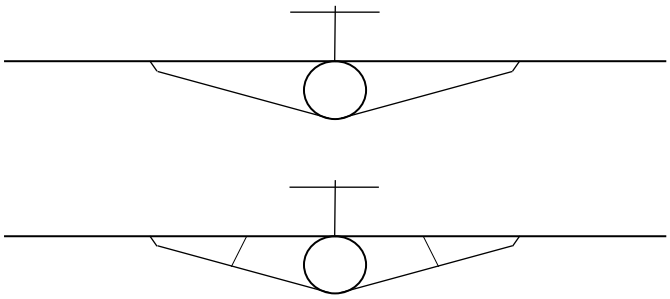

Figure 1.3: SBW (top) vs TBW (bottom) configuration

Figure 1.3 shows the difference between SBW and TBW: the first one on the top, the last one on the bottom. TBW are equipped with additional elements called juries, represented by the inclined lines between the strut and the wing on the bottom side. In this Figure, a one-jury TBW has been reported, but, generally speaking, more juries could be introduced. In literature, several works comparing SBW and TBW are present, some of which are going to be mentioned in this Section.

1.2.1. General works on SBW

The pioneer of the SBW concept is globally identified in Pfenninger, who was the first to believe in the potential of this configuration, starting to work on the topic in the 1950s

at Northtrop [13], until its retirement in the 1980s.

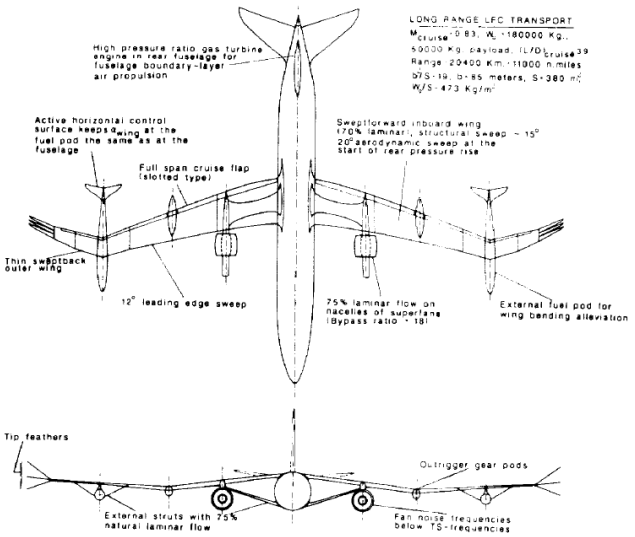

Figure 1.4: One of Pfenninger's SBW designs [14]

Figure 1.4 shows one of his SBW complex designs. In [14], he declared that the presence of the strut is needed to reduce both bending and torsional moments and deformations, and that the best choice would be to use a wide-chord low-drag laminar strut.

In 1978 Park, who worked for Boeing, studied a short-haul SBW configuration to quantify eventual fuel savings [15]. The buckling problem for the strut was adressed, concluding that, in order for the strut to not buckle, an increase of thickness was necessary, causing an increase in its parasite drag. It was observed that the wing weight does not diminish so much and that the induced drag reduction is compensated by the strut parasite drag. Comparable block fuel consumptions for CTW and SBW were found. Some concerns were expressed for the type of junction at the strut-wing attachment and its influence on flutter velocity. In the same year, another work for Boeing was published by Kulfan et al [16]. The most interesting outcome was that the statistical formulas used at that time to estimate the aircraft weights were found to be inaccurate for very high AR wings, where analytical formulas were needed.

Almost in the same years, also NASA showed interest in the configuration. In [17] a comparison was studied between CTW and SBW baseline and optimized configurations, to estimate the savings in terms of range. For both configurations, the optimized version required a high AR. The SBW resulted in a more convenient solution, because the weight savings, and so the range improvements, were higher thanks to the presence of the strut.

Moreover, lifting strut were discussed and it was concluded that they are preferable with respect to non-lifting. Another comparison was made in [18]. It was stated that to realize the high L-to-D ratio, the SBW must have a higher cruise altitude with respect to CTW, which implies also lower speeds. Even if the wing weight was found to be bigger with respect to CTW due to the high AR, the efficiency increase compensates this result. However, it was concluded that the SBW would be too expensive to be built and its lower cruise speeds confirm the superiority of the CTW. Moreover, some strut-related topics were discussed. For instance, in order to address the aforementioned strut buckling issues, juries were included in the configuration. The main effect of these elements is to shorten the free length of the strut, increasing the buckling load. Thanks to the presence of the juries, the truss won't be oversized, allowing for some weight savings. Another aspect that was touched was the spanwise position of the strut-wing attachment: if too close to the wing root, this means less load alleviation and more wing weight, if too close to the wing tip, this means a longer and heavier strut.

Some decades later, several studies were conducted on the SBW and TBW at the Virginia Polytechnic. For instance, in [19] a parametric study was performed. The objective was to understand the effect of wing geometry on the structural and aeroelastic behavior of SBW and TBW. Different parameters were considered, such as: wing half-span, strut sweep angle, spanwise location of the strut-wing attachment and the number of jury members. The results compared were mainly buckling load, wing weight, natural frequencies and flutter velocity. Increasing wing span has the effect of reducing the natural frequencies and increasing the weight. It was found that wing weight and flutter velocity are optimal for a strut-wing attachment between $55 - 70\%$ of the wing span. Also the sweep angle has an important influence on the results.

In Europe, the first work regarding the SBW was produced by ONERA with the ALBATROS project [20]. Some considerations regarding the baseline configuration were reported: fuselage-mounted engines were chosen to keep as much as possible laminar flow on the wing, this leads to a t-tail. Also in this work some studies regarding the strut spanwise position resulted in an optimal range between $50 - 70\%$ of wing span. Since no juries were considered, buckling was an inssue. It was suggested to create a curved strut such that it becomes straight for positive lift and buckles without the risk of touching the lower skins of the wing for negative lift. Drag interference between wing and strut was treated, concluding that the higher the vertical offset, the smaller the drag. Some divergence problems were highlighted and solved increasing strut thickness, meaning that if the strut is too flexible, aeroelastic problems could arise.

In a more recent NASA and Boeing work, developed in the context of the Subsonic Ultra-

Green Aircraft Reasearch (SUGAR) program in response to a NASA call for sustainable aviation, [21], some advanced problems were highlighted: for these configurations (i.e. TBW) wing thicknesses are typically reduced, but this could represent a manufacturing problem; another issue related to the thickness is how to introduce all the systems needed in the wing if there is no space available; the interaction between the landing gear and the strut at the fuselage attachment must be better understood; the strut-wing attachment must be widely studied and at some point it must be certified, e.g. bird strike could be a problem for this region. A more complete set of possible issues is reported in Figure 1.5. This also helps to understand the complexity in designing this configuration.

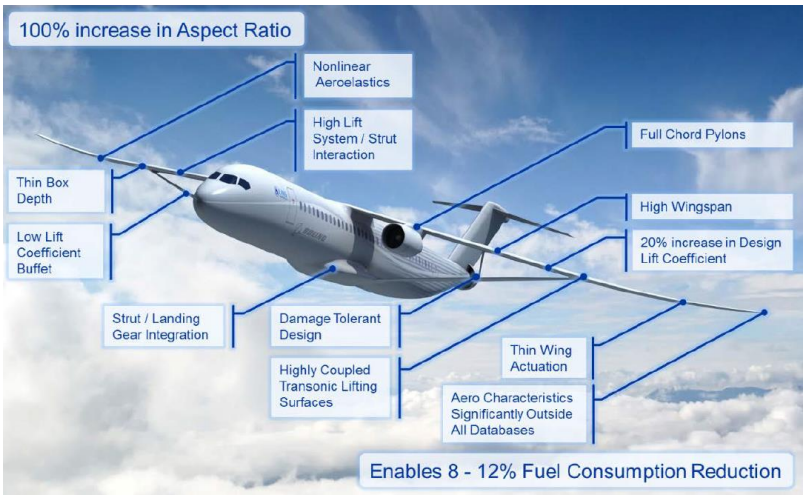

Figure 1.5: SUGAR Transonic Truss-Braced Wing potential problems [21]

Moreover, some aeroelastic problems have been found due to the control surfaces, i.e. control reversal for small spoiler deflections.

In 2022, Delavenne et al published a work regarding weight analyses of SBW during preliminary design stages [22]. Three approaches were followed increasing the fidelity of the employed methods. Only a pull-up manoeuvre and some gusts were considered as load cases. A discussion regarding wing buckling has been reported. In particular, modeling the strut only through the axial load that it is assumed to sustain, the projection of this force on the wing turns out to be a compressive force between the root and the strut attachment, meaning that this region is potentially subjected to buckling. Buckling should be considered during the sizing, but this leads to ingent increases in wing weight. Otherwise it could be neglected by correctly positioning the strut-wing attachment along

the wing span.

1.2.2. Multi-disciplinary Design Optimization

As it was already mentioned in the present work, in order to fully capture the potential of an unconventional configuration (but actually this is generally valid for all the aircrafts) all the interacting disciplines should be considered at the same time, leading to the so-called multi-disciplinary approach. This is a well-known practice.

The first MDO work related to SBW was [23]. In 1996, NASA Langley commissioned a small group of researchers at Virginia Tech's Multidisciplinary Analysis and Design Center for Advanced Vehicles a study for the feasibility of a transonic SBW using a Multi-disciplinary Design Optimization (MDO) approach. The baseline model was inspired to a Boeing 777-200IGW, a CTW and a SBW version were produced. Also advanced technologies were considered. To address buckling problems, the strut was considered inactive under compression through a telescopic sleeve, whose working principle is shown in Figure 1.6.

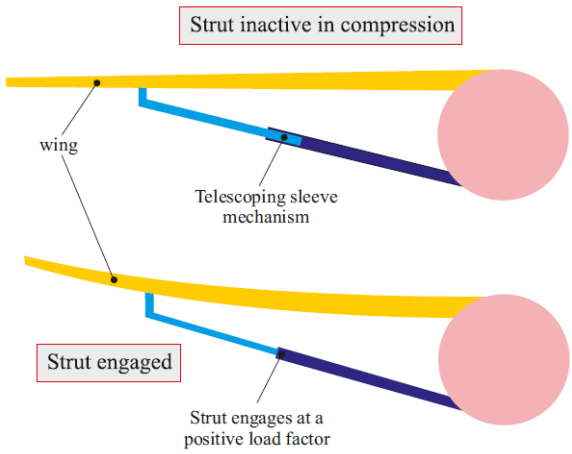

Figure 1.6: Telescoping sleeve mechanism [24]

Different positions for the engines were considered: wing-mounted and tip wing-mounted. Considering the tip wing-mounted engines in principle should help to further reduce the induced drag, however this configuration brings some criticality related to the engine out

condition. Two main solutions were considered: the first one is to apply the circulation control on the vertical tail, such that the rudder is more effective; the second one, called thrust vectoring, is to introduce a third engine in a centerline and if the engine out condition verifies it would remain the only active propeller. The problem is that introducing a third engine requires an increase in weight and it is also expensive. The optimization objective was the minimization of the Take-Off Gross Weight (TOGW). No aeroelastic analyses were included in the MDO process. The SBW appeared to be optimal, especially in the configuration with wing-mounted engines. Other studies conducted at the Virginia Polytechnic are [25] and [26], where a new method for the evaluation of the bending material has been introduced. With the partnership of Lockheed Martin, it was possible to develop a new model able to correctly capture both the bending material and the torsional stiffness of the wing, both needed for aeroelastic analyses. Some parametric studies regarding the chordwise strut-wing attachment have been reported, too. In [27] three different optimizations were produced: minimum TOGW, minimum fuel consumption, maximum efficiency. The compared models are CTW, SBW and TBW. For the minimum TOGW, both SBW and TBW presented a reduced wing weight keeping the same wing span and AR. The presence of the juries allows for a further reduction in weight due to the reduction of thickness in the wing inboard portion, as shown in Figure 1.7.

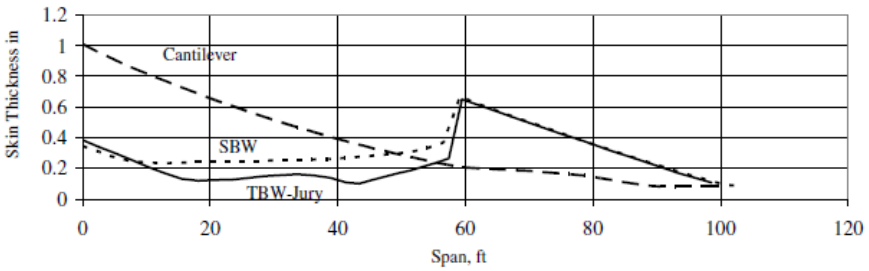

Figure 1.7: Thicknesses comparison between CTW, SBW and TBW [27]

For the minimum fuel, again SBW and TBW are the winners, because the high AR allows for an increase in L-to-D and so a decrease in fuel weight. For the maximum L-to-D, ultra high AR have been reached for both SBW and TBW, leading to an incease in wing weight with respect to the CTW. However, very important L-to-D values have been

reached. The just presented MDO studies focused on long-range missions. In [28] aircrafts for medium-range mission were analyzed. In particular different models were compared: CTW, SBW with wing-mounted engines, SBW with fuselage-mounted engines, TBW with wing-mounted engines and TBW with fuselage-mounted engines. Different levels of technology were considered as well. Two objectives were to be minimized: TOGW and fuel. Also in the case of medium-range, as it was for the long-range, SBW and TBW were superior. From the optimization analyses big strut dimensions emerged. This opens to the possibility to store the fuel not only in the wing, but also in the strut, meaning that the wing weight could be further reduced. No big differences were evidenced between SBW and TBW. In [29] the same analyses as before were enriched by including flutter. Some weight penalty appeared because of the flutter constraint. The structures were pre-stressed but the computed flutter analyses were linear. It is stated that if the structures results to be enough stiff, negligible differences between linear and nonlinear flutter analyses are expected. MDO has been applied in the SUGAR project in [30].

More recent MDO works are [31] and [32]. In the latter, both SBW and Hybrid Wing-Body (HWB) are studied. Its aim is mainly to offer a guide for the approach of unconventional configurations through a Multi-fidelity MDO. The need to include advanced aerodynamic analyses starting from the preliminary design is highlighted.

2 | Aeroelastic model

In this Chapter, the process that has brought to the studied model is reported. The first part is dedicated to some design considerations: which is the baseline aircraft, how it has been modified in order to accomodate the strut and which are the modeling choices adopted. The second part reviews the followed workflow, the tools used to generate the model and its verification along with design issues. The final part focuses on a possible solution and consequent model update.

2.1. Conceptual design considerations

The present thesis originates from a work developed by ONERA and ISAE-SUPAERO inside the U-HARWARD project. They generated a Strut-Braced Wing (SBW) aircraft model following the approach presented in [31], which can be considered as the starting point. The reasons why this unconventional configuration has gained interest have already been discussed in Section 1.1. Recalling them briefly: reducing the induced drag is an effective way to reduce consumptions and emissions. In order to do that, the wing Aspect Ratio (AR) can be increased. However, this implies an increase in wing weight due to the large reached bending moment, withdrawing the benefits of having such a high AR. A way to alleviate the wing bending loads is to introduce a strut that connects the fuselage to a certain span of the wing. In this way, when the wing bends, it is partially restrained by the strut. This leads to an overconstrained system, which is intrinsically complex. Moreover, being the wing very flexible, aeroelasticity plays a fundamental role. The model presented and studied is therefore an aeroelastic model, which allows to perform classic aeroelastic analyses to investigate the behavior of this unconventional configuration.

2.1.1. Baseline model

In order to choose a baseline aircraft, a design mission must be fixed. In this case, as stated in [31], the main requirements are:

- a range of 7400 [km];

- $\sim$ 200 passengers;
- $M_{cruise} = 0.78$;
- $M_{dive} = 0.89$;
- for the engines, the Maximum Take-Off Thrust has been fixed to 134 [kN];
- a fuel weight of 18600 [kg] has been selected.

These data more or less correspond to the ones of the Airbus A321-LR, which has been identified as the reference aircraft.

2.1.2. Introduction of the strut

After having defined the baseline model, being it a Classical Tube and Wing (CTW), it must be modified into its SBW version. Some considerations are needed. First of all, in order to increase the AR, the wing is stretched, as can be understood looking at the wing values in Table 2.1.

	A321-LR	SBW	Unit
Fuselage Length	44.51	44.38	m
Fuselage Width	3.95	4.08	m
Wing Span	34.1	55.13	m
Wing Surface	126	161.8	m^2
Wing AR	9.23	19	-
Wing Sweep	-	19	deg
HTP Span	12.45	12.44	m
HTP Surface	30.75	35.83	m^2
HTP AR	5.04	4.31	-
VTP Span	5.87	6.88	m
VTP Surface	22.3	33.93	m^2
VTP AR	1.55	1.4	-

Table 2.1: Geometrical values of baseline configuration A321-LR and its SBW version

It is then translated from the lower to the upper part of the fuselage, becoming a high wing, such that the strut can be introduced. Moreover, the reference aircraft is equipped

with twin wing-mounted engines. Since wing-mounted engines could represent a problem for the strut, because of some potential interference during flight, it has been chosen to translate them in the rear part of the fuselage, meaning that fuselage-mounted engines have been chosen. The presence of the propellers near the tail represent a potential issue for the Horizontal Tail Plane (HTP). For this reason, it has been translated in the upper part of the Vertical Tail Plane (VTP), becoming a T-Tail. Another important aspect regarding the strut is that a lifting strut has been chosen, accordingly to [17].

2.1.3. Modeling choices

There are three main differences between the present work and the one reported in [31].

1. The wing-strut attachment: in [31] it was modeled through a sleeve aligned with the wing Elastic Axis (EA) that allows the strut to be inactive in compression, in order to avoid buckling problems or an increase in the strut weight still related to buckling. In this work, the strut has been considered connected to the wing by means of a double hinge: one along the fuselage direction, one along the vertical direction. This means that neither the out-of-plane nor the in-plane bending moment can be transmitted from the strut to the wing. Torsional moment is allowed, but the strut is attached to the EA of the wing, meaning that additional torque that could be gained by attaching the strut to the wing rear or front spar is not considered. Actually, some sensitivity analyses will be performed in Chapter 4. While in [31] the strut was considered to be active only for tensile loads, i.e. positive lift, here it is active also under compression. This leads to a significant conceptual difference between the model here reported and the one obtained in [31]. Of course, an increase in weight is here expected.

2. The loads sustained by the strut: in [31] the strut has been sized considering only axial tensile loads. Actually, since a lifting strut has been considered, all the loads should be present for the sizing process. In particular, also shear and bending due to the lift play an important role. Therefore, in the present work, the strut sizing process is the same of the wing, where, depending on the structural concept considered, the single components of the wingbox are sized basing on the maxima stresses (both σ and τ) that they are able to support. For instance, if a semi-monocoque concept is applied, the section is assumed to be composed by skins, spar webs, spar caps and stringers. The formers function is to sustain torsion, in-plane and out-of-plane shear, the latters one is to sustain axial loads (both tension and compression), in-plane and out-of-plane bending.

Since

$$\sigma = \sigma(N, M_{bending_1}, M_{bending_2}); \tag{2.1}$$

$$\tau = \tau(M_{torque}, T_1, T_2) \tag{2.2}$$

skins and spar webs are sized such that enough material guarantees $\tau \leq \tau_{allowable}$, while spar caps and stringers such that $\sigma \leq \sigma_{allowable}$.

3. The load cases for sizing: in [31] the wing was sized thorugh a 2.5g and a -1g manouvre, while the strut, basing on the aforementioned considerations, was sized only thorugh the 2.5g. It is not specified in which flight points these load cases were considered. In the present work, the set of sizing manoeuvres will be presented in Table 2.5, and no distiction was made for wing and strut sizing, meaning that the same set of manoeuvres sized both the structural components. As already stated, this reasonably leads to a difference in the estimated weights.

2.2. Model generation and verification

In this Section a recipe-like approach for the model generation will be followed: first of all, the list of the *ingredients* is presented, i.e. software, starting geometry and verification method. Then the procedure, along with potential issues, are reported.

2.2.1. Employed tools

Software

The model has been generated through NeoCASS (Next generation Conceptual Aero-Structural Sizing Suite) [4] [5], an open-source code developed at Politecnico di Milano. Generally, the conceptual design of commercial aircraft is widely influenced by available datasheets and statistical-based approaches. This *modus operandi* brings out at least two problems: the first is that basing the weight estimations on statistical formulas completely excludes the presence of the airframe in this design phase, which, in turns, avoids any aeroelastic considerations. Consequently, aeroelasticity must be recovered in a successive design stage. This means that if some instability is found, some time must be spent in order to go back at the previous stage and correct the model. The second is that for unconventional configurations, such as the Strut-Braced Wing (SBW), which is the main topic of this work, no reliable data are available, introducing an important level of uncertainty in the first phases of the project. Moreover, an unconventional configuration such as the SBW is highly flexible. In such cases, aeroelasticity is particularly important, because some non-expected behaviors can occur, meaning that the earlier it is considered,

the more effective the design is. NeoCASS was mainly developed as a solution to these problems. Indeed an aeroelastic model is generated at the conceptual design stage, allowing to gain knowledge on the aeroelastic aircraft behavior yet at the beginning of the project.
The code is composed by different modules. A layout of the software is reported in Figure 2.1, while a brief review of its main features is given below.

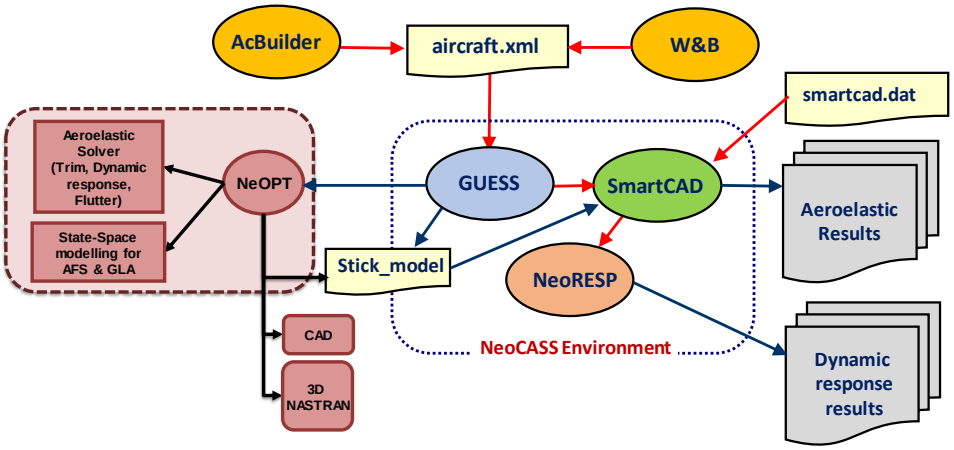

Figure 2.1: NeoCASS layout

- AcBuilder is the graphical editor, through which it is possible to visualize the aircraft shape and payload. It requires the geometrical data for each aircraft component: fuselage, wing, horizontal and vertical tail, engines, canard and some other. More data to be included are related to fuel, which is stored in the wing, and the remaining payload, which is composed by the on-board systems, the number of passengers and their weight, the baggages and the crew. Structural and aerodynamic meshes are defined, along with material and structural concept implemented for each component (e.g. semi-monocoque for lifting surfaces).

- GUESS is the module dedicated to sizing. It receives as input the file generated by AcBuilder. Then, it needs the set of manoeuvres that will be used to size the aircraft. NeoCASS allows the user to choose a set of pre-defined 35 manoeuvres, which are required by the EASA Certification Specifications (CS). In the case at hand, the CS-25 have been used. The aerodynamic loads are applied through VLM. Finally, the mass configurations can be defined by choosing an appropriate percentage of payload, in terms of fuel, passengers and baggages. The sizing is an iterative process.

Once at convergence, the result is a stick model, where each element is a beam element sized following the fully-stressed design. A distribution of stiffness and mass is therefore obtained even in the conceptual design stage.

- SMARTCAD. The aeroelastic model has been obtained, and it is ready to be processed. In this module several analyses can be computed, e.g. modal analysis, static aeroelastic analyses such as aeroelastic trim and divergence, flutter.
- NeoRESP is a solver used for dynamic response analyses, such as gust analysis, response to command deflections and response to external loads.
- NeOPT is the optimizer [6] [7]. Consequently, it can be used to correct the sizing obtained from GUESS. Indeed, if semi-monocoque structural concept is chosen, GUESS defines a symmetric wingbox where the only three unknowns are skin thickness, spar thickness and stiffeners area. This leads to an incomplete description of stick model structural properties, because, due to symmetry, couplings are not taken into account. On the contrary, NeOPT allows for a more accurate section description. Indeed, a Finite Element solver is used in each section, and up to ten separate variables can be defined, enriching each element stiffness and mass matrices. The optimization problem is composed by an objective function that must be optimized, which typically is the minimization of the semi-wingbox mass, and at the same time a set of constraints must be satisfied (e.g. buckling and failure constraints). The design variables that satisfy the problem are the optimization outputs. The number of the unknwons are user-dependent. Indeed, the semi-wingbox is subdivided in spanwise direction into patches, which are wing sectors in which the section is assumed to be constant. For instance, if 4 patches are chosen, the first sector is described by the first section, the second sector is described by the second section, and so on, meaning that only 4 sections are needed to entirely characterize the wingbox. Each section is then defined by different parameters, e.g. a section with 7 parameters is defined by: thickness of upper and lower skins, thickness of front and rear spar webs, thickness of the spar caps, thickness of upper and lower stringers. Therefore, in the considered case the number of unknowns will be 4 patches $\times$ 7 parameters $=$ 28 design variables. Also the material can be chosen.

Geometry

The starting geometry has been produced by ONERA and ISAE-SUPAERO following the approach presented in [22] and [31]. Figure 2.2 shows the SBW configuration obtained in AcBuilder. It must be pointed out that AcBuilder is not a CAD, therefore the proportions

are not entirely realistic.
As one can notice, all the features explained in Subsection 2.1.2 are present: stretched high wing, fuselage-mounted engines, T-Tail and, of course, the presence of the strut.

Table 2.2 shows the main geometrical values chosen for the strut. It is a very slender strut with almost constant chord. As reported in the Table, it is attached to the wing at 65% of wing semi-span. Comparing the strut sweep with the wing sweep, the latter being reported in Table 2.1, as can be noted also from the top view of Figure 2.2, the strut completely falls inside wing surface. The rationale behind this consideration will become clear later.

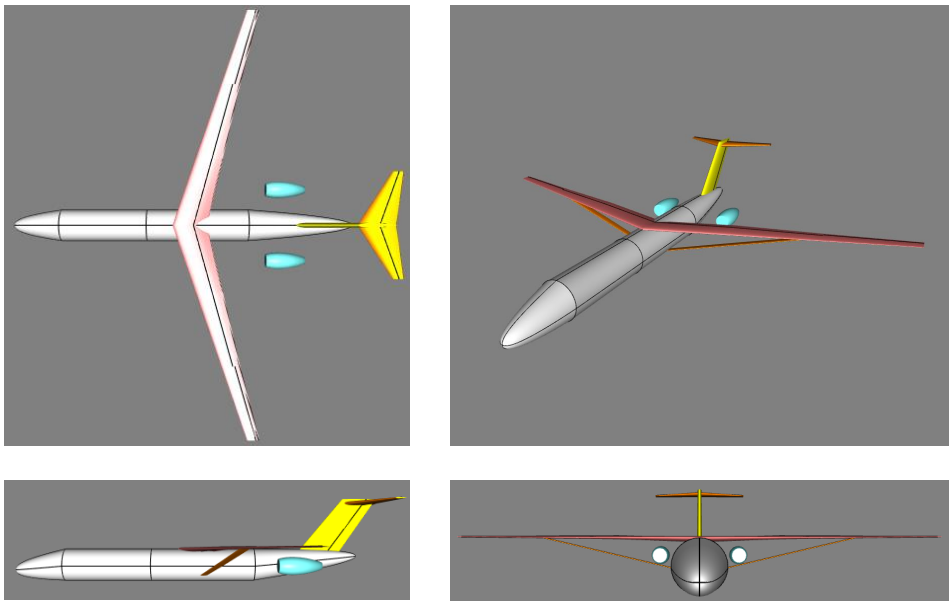

Figure 2.2: ONERA SBW representation in AcBuilder

	Value	Unit
Strut Span	34.5	m
Strut Surface	32.4	m^2
Strut AR	36.73	-
Strut Taper	1.15	-
Strut Sweep	12.5	deg
Strut Attachment to Wing	65%	-

Table 2.2: Geometrical values of SBW's strut

The material used in this phase is an Aluminium Alloy AL7075-T6, whose characteristics are reported in Table 2.3.

	Value	Unit
E	72	GPa
$\boldsymbol{\nu}$	0.3	-
G	$\tilde{2}7.7$	GPa
$\boldsymbol{\rho}$	2800	$\frac{\text{kg}}{\text{m}^3}$
$\boldsymbol{\sigma_{yield}}$	430	MPa

Table 2.3: Aluminium Alloy AL7075-T6

Verification method

In order to verify the sized model, both linear and non-linear trim analyses have been performed. The need to compute also nonlinear analyses will be explained in Chapter 3. The idea to verify the model was to check aircraft deformation under the condition with highest dynamic pressure, i.e. dive condition, reported in Table 2.4.

	M [-]	h [m]	N_z [g]
Dive condition	0.89	6760	1

Table 2.4: Definition of dive condition

2.2.2. Procedure

Still following the recipe-like parallelism, now that all the *ingredients* have been discussed, it must be understood how to use them. Since the procedure is iterative and somewhat complex to be comprehended, the main steps are presented in form of Algorithm 2.1 and schematically in Figure 2.3.

Algorithm 2.1 Procedure for model generation and verification

1: Establish geometry.
2: Give geometry as input to AcBuilder, which stores it in a dedicated file.
3: Give AcBuilder file as input to GUESS, which sizes the model.
4: Compute the trim analyses in dive with SMARTCAD, for verification purpose.
5: **if** Verification is satisfied **then**
6: Exit.
7: **else if** Issues have been found **then**
8: Go to the next step.
9: **end if**
10: Correct the sized model with NeOPT.
11: Go back to step 4.

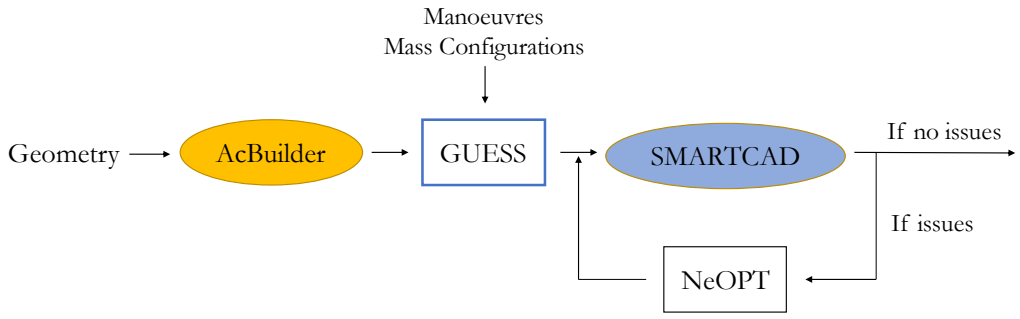

Figure 2.3: Procedure for model generation and verification

GUESS sizing

As previously anticipated and shown in Figure 2.3, in order to size the aircraft, some additional informations are needed.
The considered manoeuvres are summarized in Table 2.5. It should be noted that no unitary negative load factor manoeuvres are present, because, as already stated, GUESS generates a symmetric wingbox.

	ID	V	h [m]	N_z [g]
Max N_z	1	VD	0	2.5
Max N_z	2	VD	6760	2.5
Max N_z	3	VC	0	2.5
Max N_z	4	VC	6760	2.5
Cruise	5	VF	0	2
Gust	6	VF	0	1
Sudden pitch control	7	VA	0	1
Sudden pitch control	8	VC	0	1
Sudden pitch control	9	VD	0	1
Sudden pitch control	10	VA	0	2.5
Sudden pitch control	11	VC	0	2.5
Sudden pitch control	12	VD	0	2.5
Sideslip at max rudder	13	VA	0	1
Sideslip at overswing angle	14	VA	0	1
Sideslip	15	VA	0	1
Sideslip at max rudder	16	VS	0	1
Sideslip at overswing angle	17	VS	0	1
Sideslip	18	VS	0	1
Sideslip at max rudder	19	VA	0	1
Negative sideslip at overswing angle	20	VA	0	1
Negative sideslip	21	VA	0	1
Negative sideslip at max rudder	22	VS	0	1
Negative sideslip at overswing angle	23	VS	0	1
Negative sideslip	24	VS	0	1
Aileron max	25	VA	0	1
Aileron	26	VA	0	0.67
Negative aileron max	27	VA	0	0.67
Aileron max	28	VA	0	0.67
Gust	29	VC	0	1
Gust	30	VC	4573.5	1
Gust	31	VD	0	1
Gust	32	VD	4573.5	1
Tail down	33	VFLAND	0	0.79
Tail down MTOW	34	VFLAND	0	1
One egine out	35	VCLIMB	0	1

Table 2.5: EASA CS-25 sizing manoeuvres

Three mass configurations have been defined, as shown in Table 2.6.

	Passengers	Baggages	Fuel
MTOW	100%	100%	50%
MZFW	100%	100%	0%
OEW	0%	0%	0%

Table 2.6: Mass configurations

For the presented geometry, a wrong estimation of the torsional stiffness has been found from GUESS sizing. In order to correct the stiffness distribution, NeOPT has been exploited.

Optimization problem

The optimization problem that has been solved is represented in Equation 2.3.

$$\min_{x_i} f(x_i) \quad \text{such that} \quad constr(x_i) \leq 0 \tag{2.3}$$

where the design variables x_i are:

- thickness of upper skins;
- thickness of lower skins;
- thickness of front web;
- thickness of rear web;
- thickness of spar caps;
- thickness of upper stringers;
- thickness of lower stringers.

The objective function f to be minimized is the semi-wingbox mass.
The set of constraints *constr* are:

- structural constraints, i.e. no buckling and no failure of the components is required;
- aileron efficiency $\geq 30\%$.

The torsional stiffness increase is driven by aileron efficiency constraint.
The problem has been solved as a two-step optimization: the first one was dedicated to

the wing, the second one to the strut, meaning that at the end both wing and strut have been optimized. A Safety Factor (SF) of 1.5 has been applied to all the constraints.

Verification results

A linear trim analysis in dive (Table 2.4) has been computed for the optimized model and the related results are shown in Figure 2.4 and Figure 2.5.

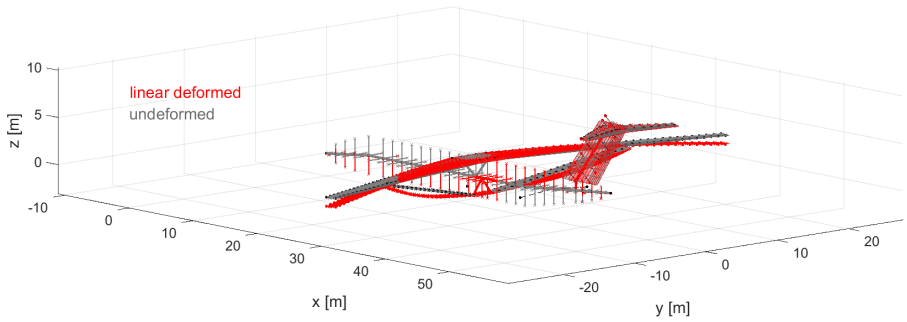

Figure 2.4: Linear trim in dive

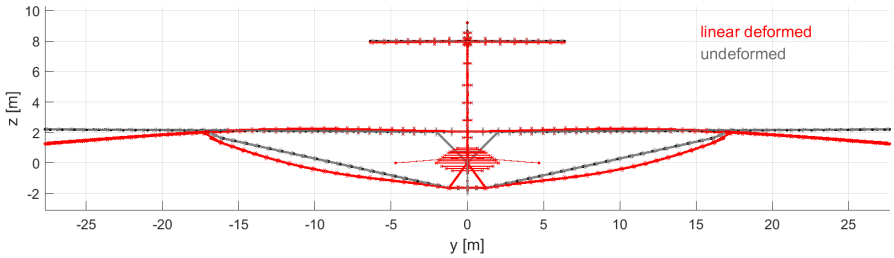

Figure 2.5: Linear trim in dive (front view)

An unexpected deformation has been obtained: as one can notice, the wing bends downward. A possible explanation for this fancy behavior could be the following. A lifting strut has been chosen. However, the starting strut is very slender, with a small chord and a small thickness. This implies that it is very flexible. The aerodynamics due to the lift, jointly with the presence of the wing, at this high pressure flight point (i.e. dive), loads a

strut with very low stiffness, leading to high deformations with the shape reported in the Figures. Being the wing attached to the strut, it is dragged down.
Also the nonlinear version of the same analysis has been computed, but the results are even worse and have been omitted for clarity.

2.3. Model update

A way to solve the problem described above consists in re-designing the strut. Some changes have been introduced:

1. the chord has been increased and is no longer constant;
2. the attachment of the strut to the fuselage has been translated towards the tail, leading to a change in strut sweep, which no longer falls inside the wing surface, as seen in Figure 2.6. This should help to partially increase wing torsional stiffness;
3. the inboard portion of the strut is horizontal, in order to reduce the strut oblique portion length, for buckling considerations (i.e. the smaller the length under compression, the higher the buckling load).

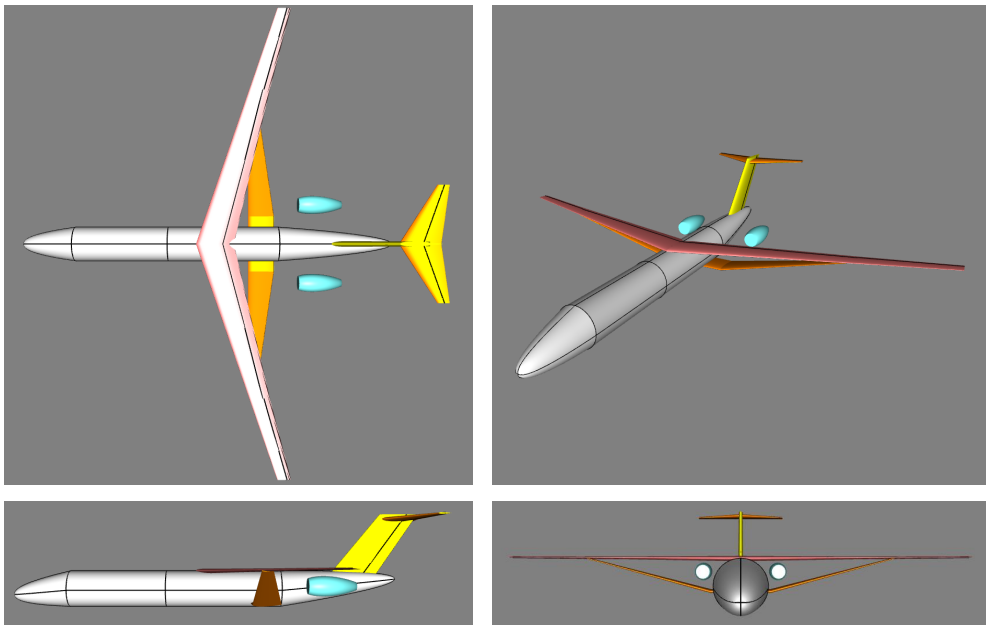

Figure 2.6: Updated SBW representation in AcBuilder

Table 2.7 shows some geometrical values for the updated strut. Recalling Table 2.2, one can notice that the position of the wing-strut attachment hasn't changed.

	Value	Unit
Strut Span	34.5	m
Strut Surface	80	m^2
Strut AR	14.9	-
Strut Taper Kink	1	-
Strut Taper Tip	0.3	-
Strut Sweep Inboard	0	deg
Strut Sweep Outboard	-1	deg
Strut Attachment to Wing	65%	-

Table 2.7: Geometrical values of updated SBW's strut

In order to account for the geometry updates, the path presented in Section 2.2.2 can be extended as shown in Algorithm 2.2 and Figure 2.7.

Algorithm 2.2 Updated procedure for model generation and verification

1: Establish geometry.
2: Give geometry as input to AcBuilder, which stores it in a dedicated file.
3: Give AcBuilder file as input to GUESS, which sizes the model.
4: Compute the trim analyses in dive with SMARTCAD, for verification purpose.
5: **if** Verification is satisfied **then**
6: Exit.
7: **else if** Issues have been found **then**
8: **if** Optimization has been chosen **then**
9: Go to line 14
10: **else if** Re-design has been chosen **then**
11: Go to line 16
12: **end if**
13: **end if**
14: Correct the sized model with NeOPT.
15: Go back to step 4.
16: Up-date geometry.
17: Go back to step 2.

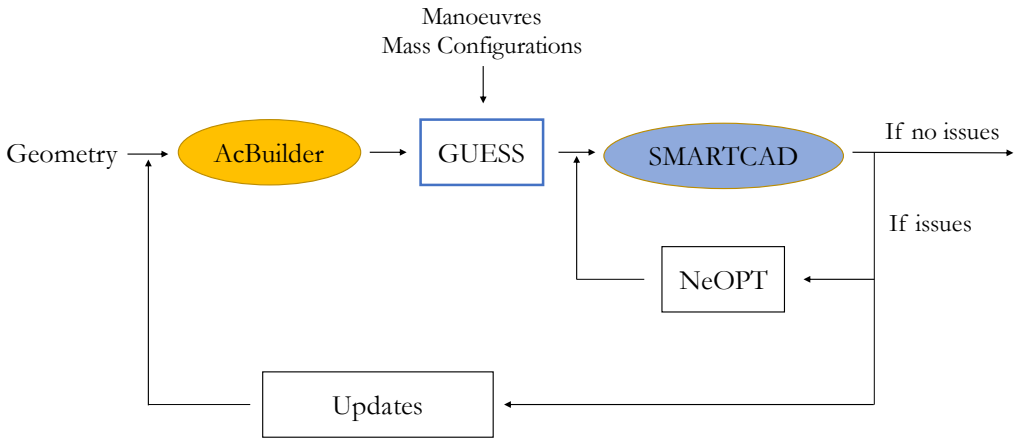

Figure 2.7: Updated procedure for model generation and verification

Also for the updated model the issue concerning the torsional stiffness has been found, therefore an optimization has been computed following the same pattern presented in the previous Section.
The results of the verification analysis are reported in Figure 2.8 and Figure 2.9. Both linear and nonlinear analyses have been computed and have given similar results.

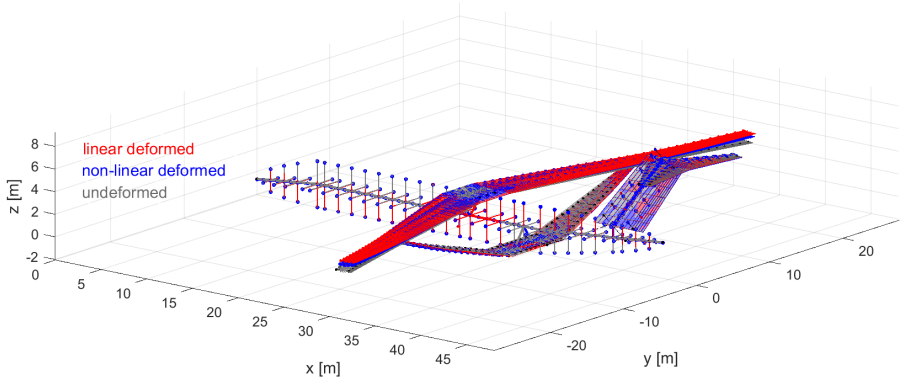

Figure 2.8: Trim in dive for updated model

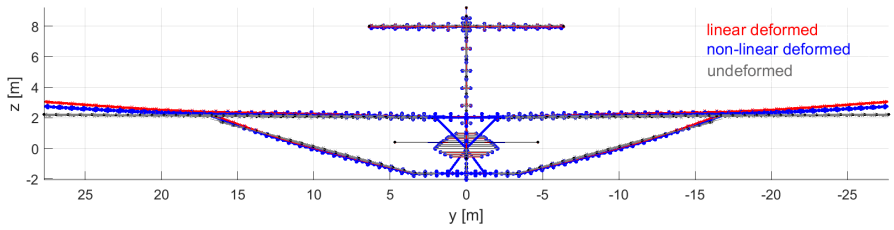

Figure 2.9: Trim in dive for updated model (front view)

A comparison of wing and strut stiffnesses between the starting model, i.e. ONERA, and the updated one is reported in Figure 2.10.

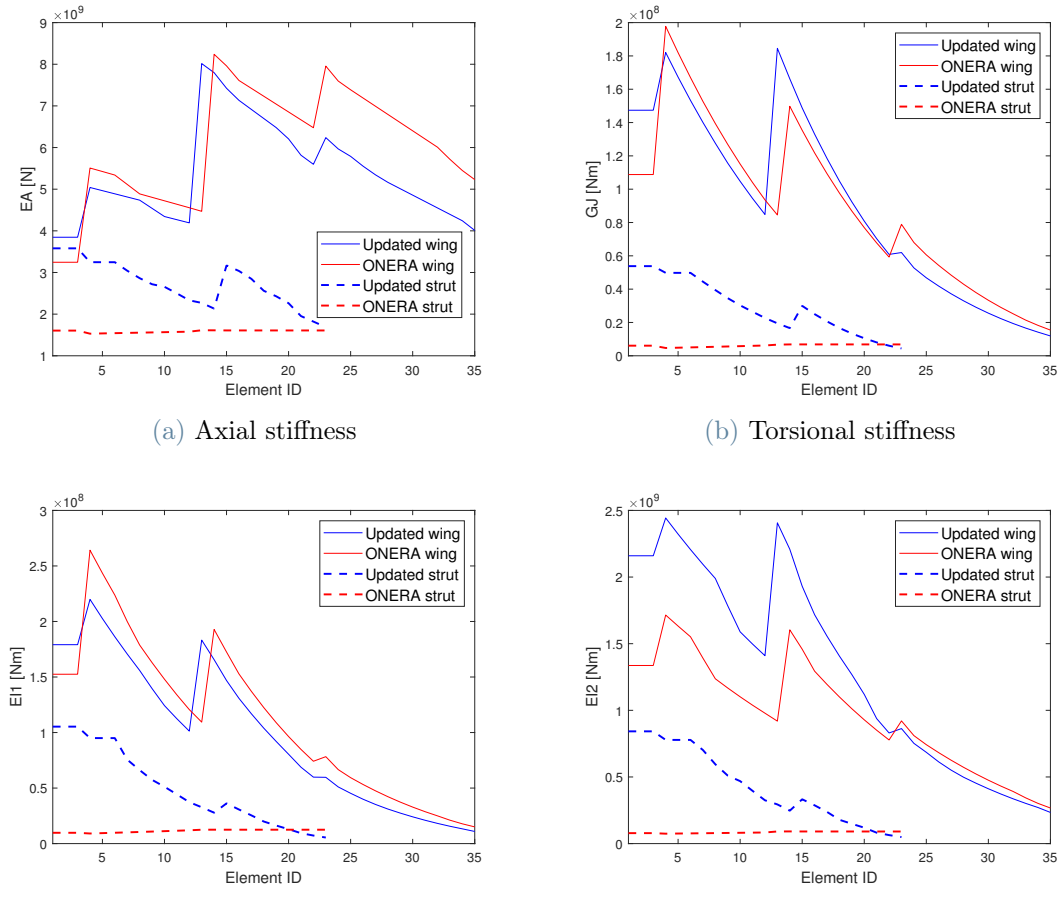

(a) Axial stiffness

(b) Torsional stiffness

(c) Out-of-plane bending stiffness

(d) In-plane bending stiffness

Figure 2.10: Comparison of wing and strut stiffnesses for starting and updated model

As one can notice, all the strut stiffnesses are consistently increased due to the augmented dimensions. Moreover, the highest impact of the updated strut on the wing happens for the in-plane bending stiffness (Figure 2.10d), due to the translation towards the rear fuselage.

Figure 2.11 and Figure 2.12 show the optimized thicknesses for the updated wing and strut, respectively, where the solution labeled as *initial* has been imposed to speed up solution convergence, therefore it is not the one obtained from GUESS.

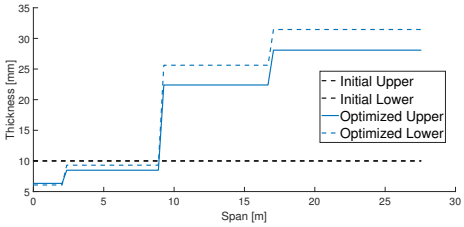

(a) Skins

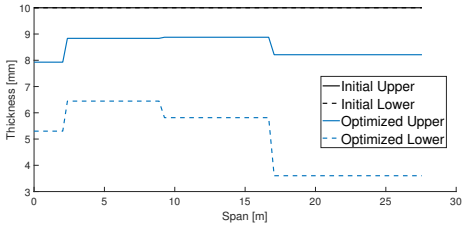

(b) Stringers

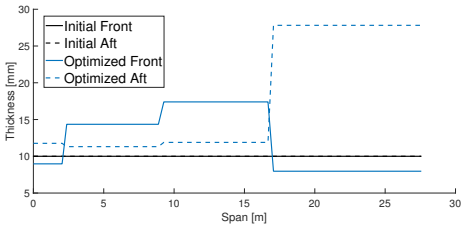

(c) Webs

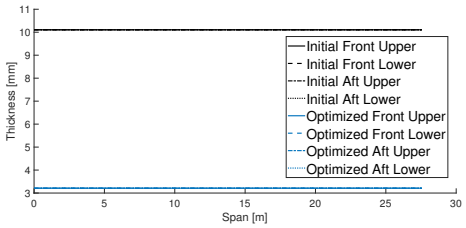

(d) Sparcaps

Figure 2.11: Wing optimized thicknesses for updated model

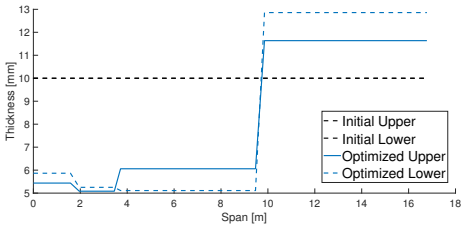

(a) Skins

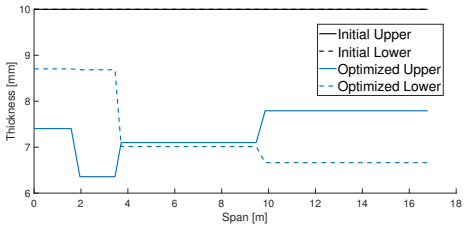

(b) Stringers

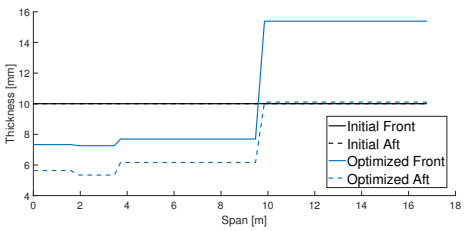

(c) Webs

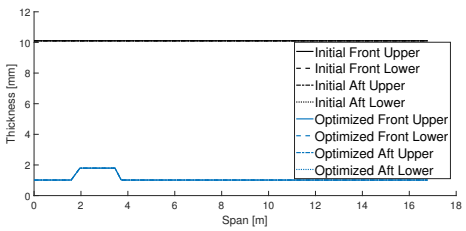

(d) Sparcaps

Figure 2.12: Strut optimized thicknesses for updated model

The weights of the updated SBW model are reported in Table 2.8, where they are compared to the original ONERA ones, where original ONERA is the model with the sleeve mechanism presented in [31]. An increase in weight is encountered, due both to model choices discussed in Subsection 2.1.3 and strut re-design.

	Updated SBW [kg]	original ONERA SBW [kg]	Δ%
MTOW	101685	85014	16.4
MZFW	83084	68719	17.3
OEW	63284	45719	27.8

Table 2.8: Comparison of weights between original ONERA and updated models

To complete the updated model characterization, an eigenanalysis has been computed. In Table 2.9 the first deformable natural frequencies are reported.

	frequency [Hz]
Mode 1	1.05
Mode 2	1.57
Mode 3	2.24
Mode 4	2.32
Mode 5	3.08
Mode 6	3.16
Mode 7	3.91
Mode 8	4.44
Mode 9	4.86
Mode 10	5.48
Mode 11	5.49
Mode 12	5.75
Mode 13	6.20
Mode 14	6.90

Table 2.9: Updated SBW natural frequencies

As one can notice, they are smaller with respect to a conventional aircraft, where e.g. the first symmetric bending mode is characterized by a $f \in [1.5 : 2]$ [Hz]. This can be explained due to the high flexibility of the considered structure. Some modes are also

very close, e.g. 10 and 11.
In Figure 2.13 it is possible to see the first three eigenmodes. They seem to be a wing symmetric bending, a wing antisymmetric torsion and a wing symmetric torsion respectively. In the second mode a contribution is given also by the tail.

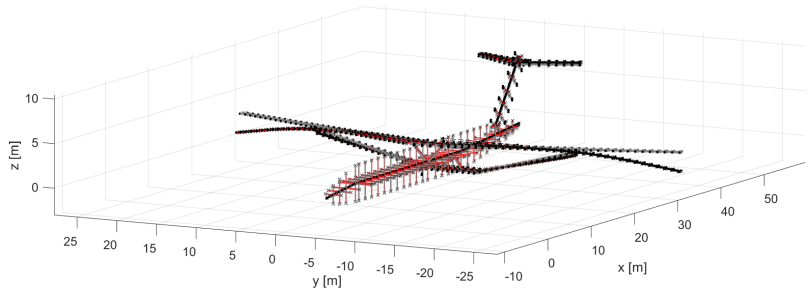

(a) Mode 1

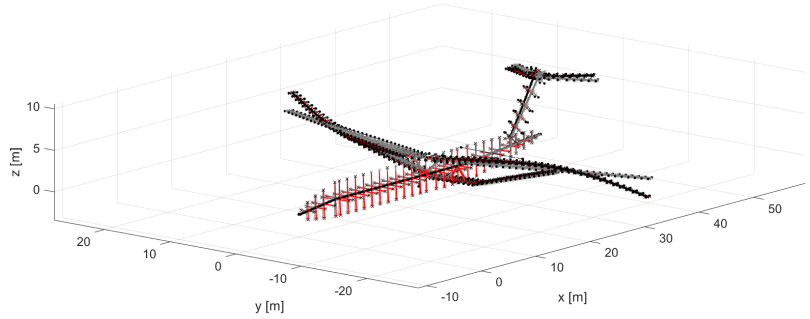

(b) Mode 2

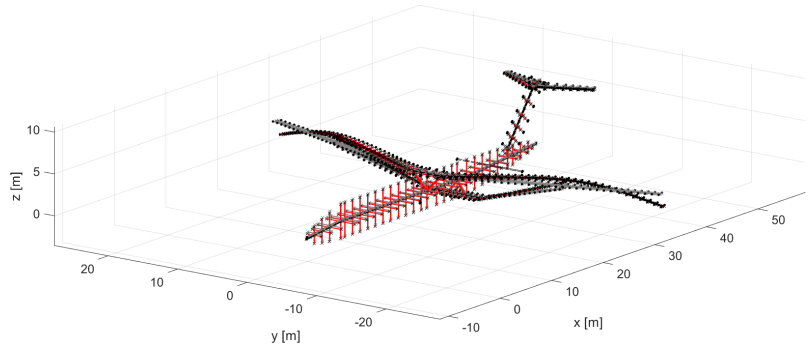

(c) Mode 3

Figure 2.13: Updated SBW modes

Comparison of SBW and CTW

It is possible to quantify bending moment reduction due to the presence of the strut, by comparing the internal actions of updated SBW and a correspondent CTW model, which was obtained sizing the very same geometry, without the strut. The comparison is shown in Figure 2.14. Also the difference in mass can be quantified, as reported in Table 2.10.

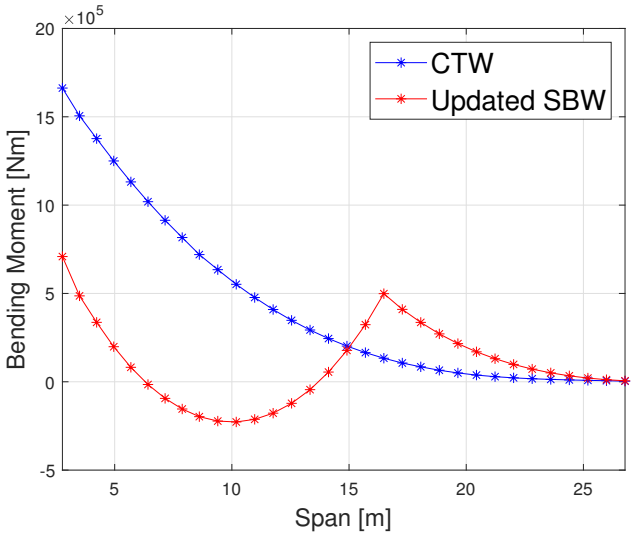

Figure 2.14: Bending moment comparison between CTW and updated SBW

	CTW [kg]	SBW [kg]	Δ%
Half Wing Structural Mass	7982	5976.4	25
Half Strut Structural Mass	-	1796.9	-
Total Half Structural Mass	7982	7773.3	2.6

Table 2.10: Structural mass comparison between CTW and updated SBW

It must be stated that the present work is considering preliminary analyses, this means that the mass difference can be even greater if an effective design for a lighter strut is considered. Moreover, this limited mass gain is somehow expected, as discussed in Subsection 2.1.3.

3 | Aeroelastic analyses

The objective of this Chapter is to give a summary of the analyses that have been computed in the present work. The results will be shown in a dedicated Chapter.

3.1. General overview of aeroelastic analyses

There are several aeroelastic analyses that can be numerically solved in order to capture the behavior of an aircraft. They are generally divided in static and dynamic analyses, where *static* means an immediate adjustment to a perturbation, while *dynamic* means that this adjustment takes some time to occur. From the structural point of view, these concepts translate in keeping (for dynamics) or descarding (for statics) inertia contributions, while from the aerodynamics one, they lead to a dependency of the aerodynamic loads both on Mach number and reduced frequency (for dynamics) or just on Mach number (for statics).
The most common aeroelastic analyses are summarized in Table 3.1, where the bold ones can be computed in NeoCASS.

Static analyses	Dynamic analyses
Trim	**Flutter**
Divergence	**Gust response**
Control reversal	**External load response**
	Buffet
	Limit Cicle Oscillation (LCO)

Table 3.1: Typical static and dynamic aeroelastic analyses

Besides the distinction between statics and dynamics, in the context of the present work another important concept must be pointed out. Indeed, as previously widely discussed, the model to be analyzed represents a Strut-Braced Wing (SBW) aircraft, with an Aspect Ratio (AR) of 19, as reported in Table 2.1. This implies that high flexibility is involved

and consequent large displacements can be reached. Under this circumstance, nonlinearity should be taken into account, because it could lead to very different outcomes with respect to the linear case. For this reason, in the present Chapter the analyses are divided in linear and nonlinear. A quick review of how they work and which are the inputs and outputs is given.

3.2. Linear analyses

In this Section, the computed linear analyses are reported.

3.2.1. Trim

Trim analyses play an important role during the conceptual design of an aircraft. First of all, they are needed to size the structure. Indeed, for each considered manoeuvre, these type of analyses have been computed in an iterative process to evaluate the internal loads that must be sustained by the aircraft. This path has been followed both for GUESS and NeOPT, i.e. the two sizing phases of the process presented in Figure 2.3. A trim analysis has been exploited also for the model verification, as reported in Subsection 2.2.1. Another interesting trim, besides the cited ones, is the one in cruise condition, which, as a rule of thumb, can be considered to evaluate if the obtained model is sized correctly. Actually, as already stated, in the present work the trim used with this purpose is the one in dive, while the cruise one is considered to have an overview of how the aircraft deforms during the longer phase in flight.
The system of equations that must be solved generally is presented in the form:

$$\boldsymbol{K}\boldsymbol{u} + \boldsymbol{M}\ddot{\boldsymbol{u}} = \boldsymbol{f}(\boldsymbol{u}, \boldsymbol{\delta}), \tag{3.1}$$

$$\boldsymbol{f}(\boldsymbol{u}, \boldsymbol{\delta}) = q[\boldsymbol{AICS}]\boldsymbol{u} + q[\boldsymbol{P}^a]\boldsymbol{\delta}. \tag{3.2}$$

Equation 3.1 reports the classical equilibrium of forces without the damping contribution, which is not known a priori, while in Equation 3.2 is specified the aerodynamic load, which depends both on structural displacements and on trim parameters. By substituting the second equation in the first one, and re-arranging it, Equation 3.3 is obtained, with the structural stiffness matrix corrected by the contribution of aerodynamics.

$$(\boldsymbol{K} - q[\boldsymbol{AICS}])\boldsymbol{u} + \boldsymbol{M}\ddot{\boldsymbol{u}} = q[\boldsymbol{P}^a]\boldsymbol{\delta} \tag{3.3}$$

The way this equation is solved depends on the constraints. Indeed, if an unrestrained condition is considered, such as the free-free constraint typical of fliing aircrafts, inertia relief could be exploited, determining the rigid body acceleration that guarantees equilibrium with the applied external loads. The deformable problem can then be solved as function of the rigid body one. Different is the case where the aircraft is grounded. Indeed, under this condition, the attitude must be imposed because no rigid motion is present, and the output is simply the solution of the deformable problem.
In Table 3.2 is reported an example of input and output for a symmetric trim, e.g. cruise, where the inputs that must be provided are the flight point definition (by means of Mach and altitude) and the load factor, which can be seen as the trim parameter. The outcomes are the Angle Of Attack (AoA, α), the deflection of the considered control surface (i.e. the elevator, δ_e) and the displacements. Particularly interesting are the vertical displacement and the torsion of the wing tip, which immediately allow to understand how the aircraft is behaving. It is also possible to directly take a look at the deformed configuration.

Input	Output
M, h, N_z	α, δ_e, $\boldsymbol{u}$

Table 3.2: Example of input and output for a symmetric trim problem

3.2.2. Divergence

Divergence is a static stability analysis. Therefore, it is presented in the form of an eigenvalue problem. Its objective is to estimate which is the limit dynamic pressure that, if reached, from a mathematical standpoint causes the singularity of the stiffness matrix, while from a physical perspective means that a finite value of force generates a huge deformation of the structure leading to a catastrophic behavior.
For sake of simplicity, only the restrained case is reported. Under this condition, the system of equations reads:

$$(\boldsymbol{K} - q[\boldsymbol{AICS}])\boldsymbol{u} = 0, \tag{3.4}$$

which is obtained as Equation 3.3 without the forcing terms.
In Table 4.3 the input and output for this type of analysis are given. As already anticipated, the outcome is the divergence dynamic pressure, which must fall outside the flight envelope of the aircraft. For Classical Tube and Wing (CTW), divergence velocity is higher with respect to the flutter one, for this reason the main aeroelastic stability analysis that is conducted is the latter. This could be no longer valid for unconventional

configurations.

Input	Output
M, h	q

Table 3.3: Example of input and output for a divergence analysis under restrained constraints

3.2.3. Flutter

Flutter is a dynamic stability analysis. As already stated for divergence, also this problem is formulated is the form of an (unconventional) eigenvalue problem. It is typically solved in frequency domain. The investigation is focused on finding the dynamic pressure, or stream velocity, such that at least one eigenvalue real part becomes negative. If detected inside the flight envelope, this phenomenon is very dangerous and must be avoided. In the conceptual design phase, for instance, an optimization problem can be solved introducing the flutter constraint. Another possibility is to design an appropriate flutter suppression system.
To derive the flutter equations, the starting point is the equilibrium of forces:

$$\boldsymbol{M}\ddot{\boldsymbol{u}} + \boldsymbol{K}\boldsymbol{u} = \boldsymbol{F}. \tag{3.5}$$

By computing a modal analysis it is possible to estimate the base of the eigenmodes needed to reduce the system. Once the reduction has been applied, a transformation in Laplace domain is required. The Laplace variable s can be transformed into its nondimensional version, i.e. $p = \frac{c}{2V_\infty}s$. The imaginary part of p is called reduced frequency and is indicated as k. The generalized aerodynamic forces are calculated through the DLM in the reduced frequency domain. Considering all these informations, including also structural damping for completeness, Equation 3.5 can be re-arranged as:

$$(-s^2\boldsymbol{M_{hh}} + js\boldsymbol{C_{hh}} + \boldsymbol{K_{hh}} - \frac{1}{2}\rho {V_\infty}^2 \boldsymbol{Q_{hh}}(k, M))\boldsymbol{q}(k) = 0. \tag{3.6}$$

This non trivial problem, where the eigenvalue s is also present inside the aerodynamic matrix in a non-polynomial way, can be solved using different techniques, e.g. the $p-k$ method.
In Table 3.4 are reported the input and output of the analysis. Of course the flight points where the analysis is computed must be provided, but also a set of reduced frequency

for the computation of the generalized aerodynamic forces, and the modal base for model reduction. The output is the so-called $V-g$ diagram, which represents the evolution of the damping factor $g = 2\frac{Re(s)}{|Im(s)}$ with velocity, for each considered eigenmode. Flutter happens when a velocity such that $g = 0$ is found. Generally, also another diagram is given as output, which is the $V-f$ one, where the evolution of frequency with velocity is reported. When flutter occurs, in general on the $V-f$ is observed a coalescence between two modes, i.e. the frequency trackings of the interacting modes tend to be the same.

Input	Output
M, h, k, modal base	$V-g$ plot

Table 3.4: Input and output for a flutter analysis

In order to have a clear knowledge of flutter behavior for an aircraft, typically more flight points are tested. There is not a unique rule to choose them, but generally the most dangerous ones are close to the corner point, i.e. where both aerodynamic pressure and Mach number have reached their maxima allowed values. The regulations require, in order to certify an aircraft, that no flutter is present inside the flight envelope, up to a velocity of 1.15VD for civil aviation. This suggests that flutter analyses should be computed for a range of velocity that reaches this prescribed value.

3.2.4. Gust

Gust response is a dynamic aeroelastic analysis very important for the sizing of civil aircrafts. Indeed, in order to efficiently estimate stiffness and mass distributions, the most critical load conditions should be considered during the sizing process. If this is true, the obtained model is able to sustain all the loads that the aircraft can encounter during its life. Choosing the conditions that generate the highest internal loads is not an easy task and in general requires to test a huge database of manoeuvres. However, since the present work focuses on just the conceptual design phase, a reduced database of flight conditions have been considered, i.e. the one suggested by the regulations and presented in Table 2.5. These are frozen manoeuvres. The regulations require to compute also gust responses, which are dynamic analyses, and add the resulting increment of internal loads to the frozen manoeuvres characterized by unitary load factor. The reason is that during flight it's common to encounter a gust, and this can lead to reach values of internal actions that fall outside the sizing database, becoming potentially very dangerous, because the structure was not sized to be able to sustain that amount of load.

The equations of gust analysis can be obtained starting from Equation 3.6. Indeed, just the forcing term must be added, which is obtained through the influence matrix that allows to evaluate the generalized aerodynamic forces due to gust, as it was due to structural displacements. The final equations are in the form:

$$\left(-\left(\frac{2V_\infty}{c}k\right)^2 \boldsymbol{M_{hh}} + j\left(\frac{2V_\infty}{c}k\right)\boldsymbol{C_{hh}} + \boldsymbol{K_{hh}} - q_\infty \boldsymbol{Q_{hh}}\left(k, M\right)\right)\boldsymbol{q}\left(k\right) = q_\infty \boldsymbol{Q_{hg}}\left(k, M\right) V_G. \tag{3.7}$$

The problem is solved in frequency domain. The result is then anti-transformed in time domain.
In Table 3.5 the inputs and outputs of the gust analysis are reported. The inputs are basically the same of the flutter analysis, but in this case they are also exploited to recover the gust shape, which, accordingly to the regulations, is a $1 - cos$. The outputs are the so-called enlarged $2D$ plots, which represent the envelope of correlated internal actions in terms of shear, bending moment and torque, considering also the presence of the gust.

Input	Output
M, h, k, modal base	$2D$ plot

Table 3.5: Input and output for a gust analysis

If some gust analysis was found to be critical, it should be included inside the sizing process. For instance, as stated in case of flutter, an optimization problem can be solved including the gust constraint.

3.3. Nonlinear analyses

The computed nonlinear analyses are trim and flutter. At the moment, NeoCASS allows to compute this type of analyses only for grounded systems. Therefore, the equations reported in the following do not include rigid body motion. For a more complete explanation, please refer to [33].

3.3.1. Nonlinear trim

Starting from Equation 3.1, considering a restrained system, one can obtain:

$$\boldsymbol{K}(\boldsymbol{u})\,\boldsymbol{u} = \boldsymbol{f}(\boldsymbol{u}, \boldsymbol{\delta})\,. \tag{3.8}$$

In order to solve this nonlinear set of equations, a linearization can be computed around the equilibrium condition:

$$\boldsymbol{K}\bar{\boldsymbol{u}} + \boldsymbol{\Delta K}\bar{\boldsymbol{u}} + \boldsymbol{K}\boldsymbol{\Delta u} = \boldsymbol{f}(\bar{\boldsymbol{u}}, \boldsymbol{\delta})\,. \tag{3.9}$$

A re-arrangement leads to:

$$(\boldsymbol{K_g} + \boldsymbol{K_m})\,\boldsymbol{\Delta u} = \boldsymbol{f}(\bar{\boldsymbol{u}}, \boldsymbol{\delta}) - \boldsymbol{f_{int}}, \tag{3.10}$$

where the geometrical stiffness matrix accounts for a correction to the material one, i.e. the classical linear stiffness matrix, due to the presence of a pre-load, or pre-stress. The summation of geometrical and material stiffness matrices defines the tangent stiffness matrix, and the equations to be solved assume the form:

$$\boldsymbol{K_T}\boldsymbol{\Delta u} = \boldsymbol{f}(\bar{\boldsymbol{u}}, \boldsymbol{\delta}) - \boldsymbol{f_{int}}. \tag{3.11}$$

Generally, to solve this problem, an incremental-iterative method is used, where a set of load steps are defined, i.e. the external load is subdivided in increments, and inside each load step an iterative process runs until the imbalance between the internal and the external loads is sufficiently small. The tangent stiffness is updated at each iteration. Since aerodynamics depends on the structural displacements, between two consequent load steps a linear trim analysis is performed around the last converged solution achieved (i.e. $\bar{\boldsymbol{u}}$), in order to update the external load. For this reason, $\boldsymbol{f} = \boldsymbol{f}(\bar{\boldsymbol{u}}, \boldsymbol{\delta})$.
Table 3.6 shows the inputs and outputs of a nonlinear trim analysis in case of symmetric manoeuvre.

Input	Output
M, h, N_z, α	$\boldsymbol{u}$, $\boldsymbol{K_T}$

Table 3.6: Example of input and output for a symmetric nonlinear trim problem

Since the model is grounded, the attitude must be provided as input. In the present work, in order to keep consistency, first a linear trim analysis has been computed in the desired flight point in order to estimate the attitude of the free-free aircraft. Then, this has been imposed to the grounded model and a nonlinear trim analysis in the same point has been conducted.

3.3.2. Nonlinear flutter

Nonlinear flutter is a conventional flutter analysis solved for each given flight point, where a nonlinear trim solution is computed in order to estimate the tangent stiffness matrix, which will be exploited to reduce the model.
Schematically, for each flight point what happens is the following:

1. a nonlinear trim is computed in order to evaluate the tangent stiffness matrix;
2. an eigenanalysis is performed leading to the reduced base;
3. the aerodynamics is updated on the deformed configuration;
4. the reduction is applied to the model containing also the correct stiffness matrix, and a classical linear flutter analysis as presented above is performed.

Inputs and outputs are the same presented in Table 3.4.

4 | Results

The results regarding the analyses described in Chapter 3 are reported. In particular, the work is divided in two main parts. The first one focuses on the model obtained in Chapter 2, here named *reference model*. The last one shows some parametric investigations. Specifically, it is studied how the changes of wing and strut material, of mass configuration, of strut geometry and of wing-strut attachment chordwise position affect sizing, trim, gust, divergence and flutter solutions.

4.1. Part I: reference model results

As anticipated, in this Section linear and nonlinear trim, gust, divergence and linear and nonlinear flutter of the reference model (from Chapter 2) are studied.
A quick recap on the main characteristics of this model can be useful.

- Material: Aluminium Alloy AL7075-T6 (see Table 2.3).
- Mass configuration: Operative Empty Weight (OEW, see Table 2.6).
- Strut geometry: straight (opposite to curved strut, which is studied in the dedicated parametric analysis).
- Wing-strut attachment chordwise position: on wing Elastic Axis (EA).

4.1.1. Trim

The flight point chosen is cruise condition, whose definition is presented in Table 4.1.

	M [-]	**h [m]**	**N_z [g]**
Cruise condition	0.78	11000	1

Table 4.1: Definition of cruise condition

Both linear and nonlinear trim analyses have been studied. The associated deformed configurations can be seen in Figure 4.1 and Figure 4.2.

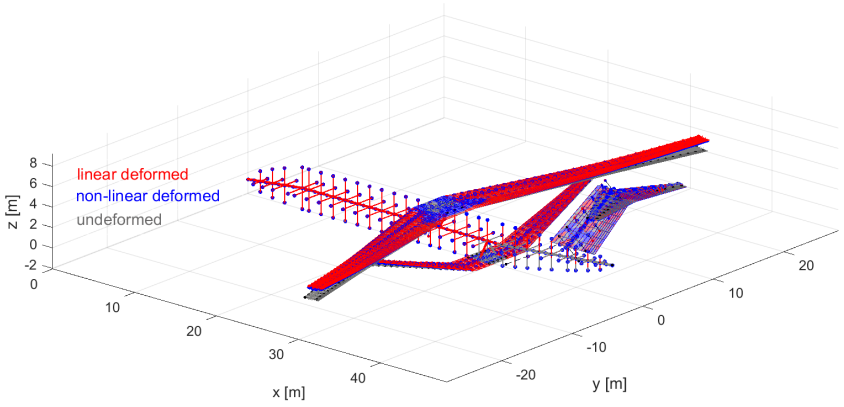

Figure 4.1: Trim in cruise for reference model

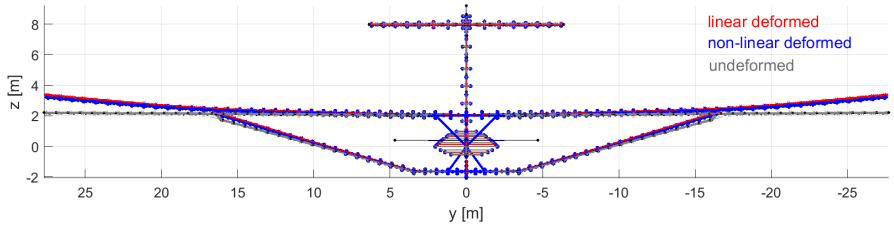

Figure 4.2: Trim in cruise for reference model (front view)

In Table 4.2 a quantitative comparison between linear and nonlinear trim analyses in cruise is reported, where the a-dimensional vertical displacement is given by the ratio of the vertical displacement and the wing semi-span.

	Linear	**Nonlinear**	$\Delta\%$
Vertical Displacement [m]	1.16	1.01	13
A-dimensional Vertical Displacement [%]	4.2	3.6	13
Torsional Rotation [deg]	-1.75	-1.6	8.5

Table 4.2: Wing tip linear vs nonlinear results for trim in cruise

As one can notice, the nonlinear results are slightly lower with respect to the linear ones, because of the presence of geometrical stiffness matrix.

4.1.2. Gust

Figure 4.3 shows the flight points considered for gust analyses. The curves connecting the dots are isoEAS.

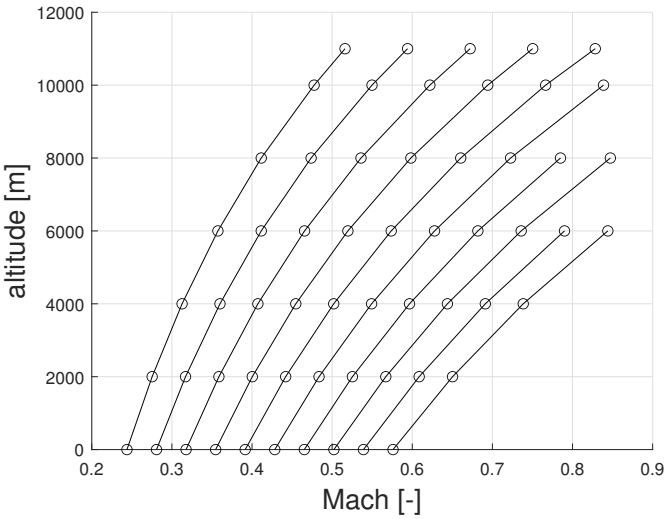

Figure 4.3: Flight points for gust analyses

In particular, for each flight point, three trim analyses have been performed varying the load factor: one with $N_z = -1$, one with $N_z = 1$ and one with $N_z = 2.5$. Wing internal actions are evaluated and the correlated shear, out-of-plane bending moment and torque are reported in the so-called $2D$ plots, one for each wing section.
Then, gust analyses are executed and the resulting loads are summed to the ones corresponding to trims with $N_z = 1$, accordingly to the regulations. The $2D$ plots are therefore enlarged. If the enlargment generates new maxima and minima, it means that some potentially critical gust manoeuvres have been found and it must be verified that the sized aircraft is still able to sustain such loads. If this does not occur, the structure must be re-sized, considering in the process also the gusts found to be critical.
The results are reported in Figure 4.4, for wing root and wing-strut attachment sections, where OL means open loop, i.e. without control laws.

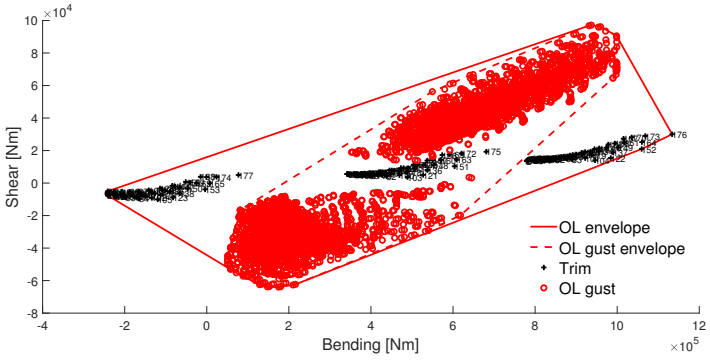

(a) Bending vs Shear (wing root)

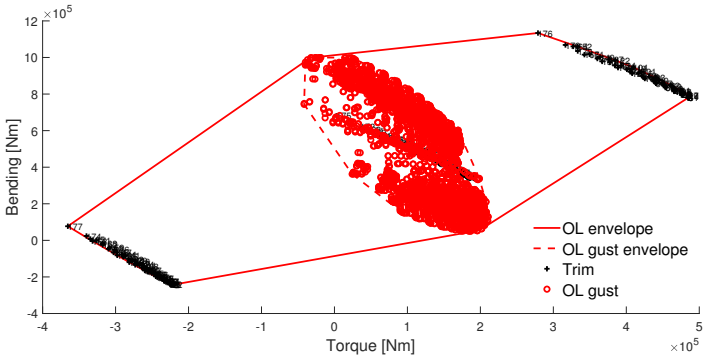

(b) Torque vs Bending (wing root)

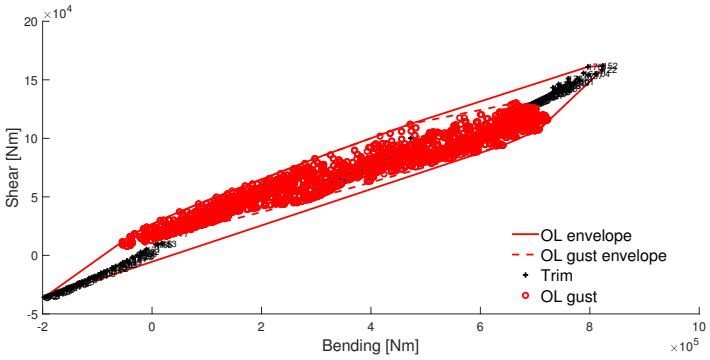

(c) Bending vs Shear (wing-strut attachment)

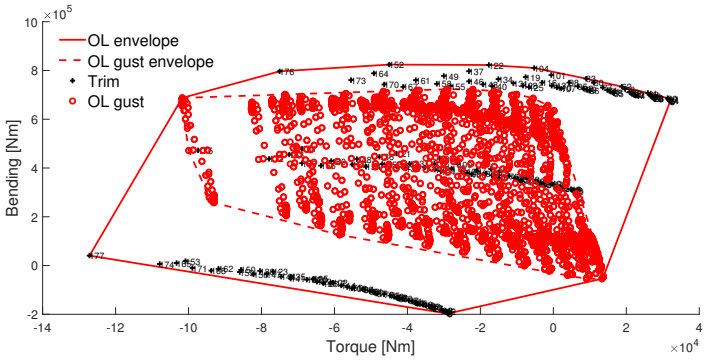

(d) Torque vs Bending (wing-strut attachment)

Figure 4.4: Wing $2D$ plots with gust

As one can notice, maxima and minima of wing root shear are due to gusts. On the contrary, bending and torque extreme values for both wing root and wing-strut attachment sections are due to trims.
It is actually possible to plot the envelope of maxima and minima due to trim and due to gust, along the wing semi-span, in order to check if and where gusts could be critical, as reported in Figure 4.5.

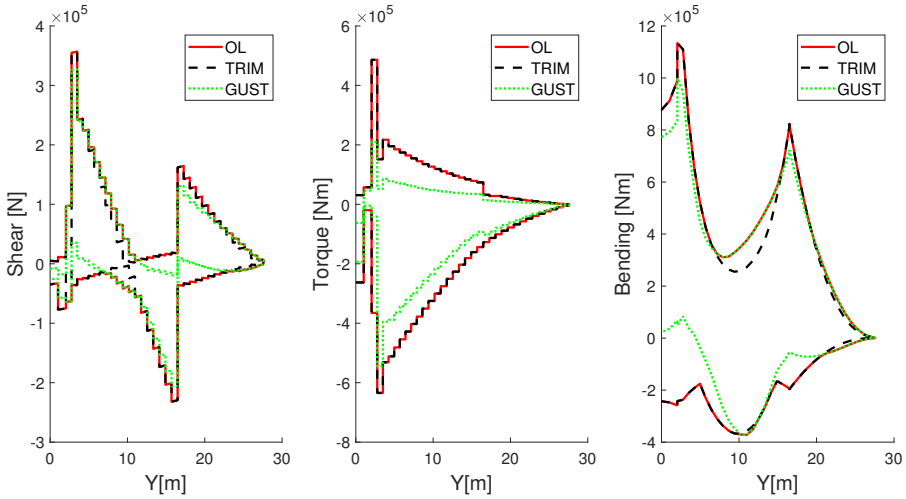

Figure 4.5: Wing maxima and minima spanwise envelopes with and without gust

The regions where the green curve exceeds the dashed black one are present both for shear and bending, where in the latter case it is particularly evident in the wing central region. However, following the approach presented in Equations 2.1 and 2.2, it has been verified that these loads do not generate stresses that exceed the allowables, meaning that no critical gust has been found. Therefore there is no need to update the sizing.

4.1.3. Divergence and flutter

Being both divergence and flutter stability analyses, they are presented together. Both the analyses have been computed in the same flight points, reported in Figure 4.6 as red diamonds labeled with 1, 2 and 3. The standard flight envelope of the studied aircraft is represented in blue, where the dashed blue line is the dive EAS velocity, i.e. the maximum velocity that the aircraft can reach during flight. The regulations require to demonstrate the absence of flutter up to a velocity that is 15% greater than the dive one, for civil aircrafts. Considering this, the red region has been introduced, which takes into account the flight envelope extension in order to reach VEAS = 1.15VD, represented by the dashed red line. In principle, flutter should be studied along this curve. Since for the

aerodynamics DLM is used, the vertical black line poses a limitation for Mach number. However, at the corner point, which is the flight point where both the highest dynamic pressure and the highest M are experienced, the red line exceeds M = 1. For this reason, the diamond point 3 has been translated from the red to the black dashed line, which represents the condition VEAS = 1.05VD.

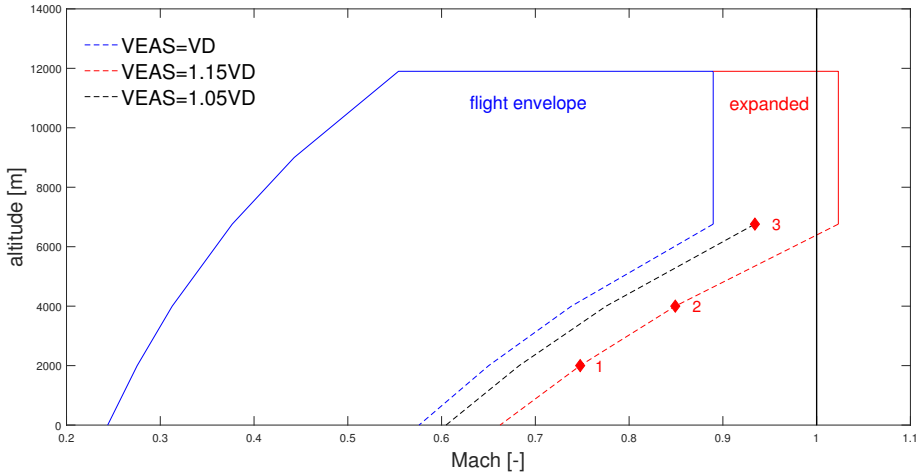

Figure 4.6: Flight points for divergence and flutter analyses

Moreover, for each diamond point, two different load factors have been assumed: $N_z = 1$ and $N_z = 2.5$. In order to understand this choice, it must be recalled that NeoCASS allows to compute both linear and nonlinear flutter analyses (while for divergence, at the moment only linearity can be considered). Nonlinear anlyses depend on attitude, as stated in Chapter 3. The change in load factor generates, for the same flight point, a change in attitude, possibly leading to different flutter results, hence the choice of different N_zs.

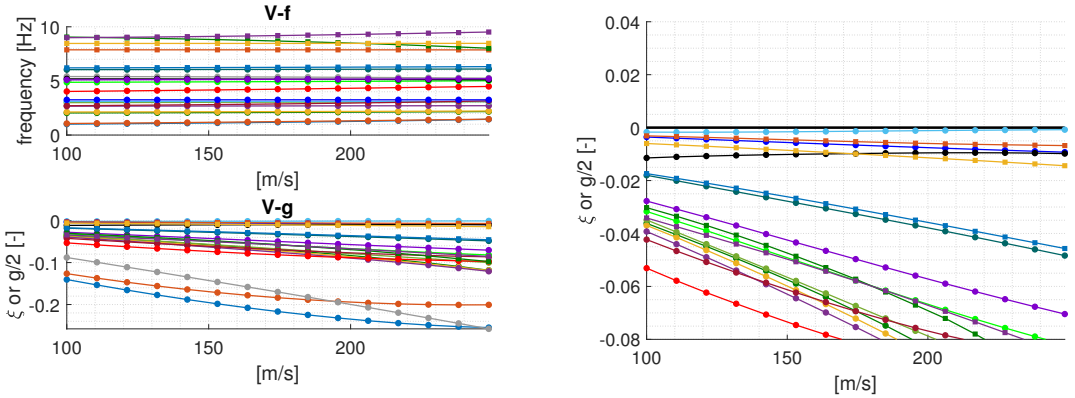

(a) V-f and V-g

(b) V-g zoom

Figure 4.7: Linear flutter results for point 1 and $N_z = 1$

Figure 4.7 shows an example of the results obtained in flutter analyses. Since Figure 4.7b is much clearer with respect to Figure 4.7a to check if flutter occurs, from now on, in the present work, only figures of this type are reported concerning flutter results.

Figure 4.8 shows the results of linear and nonlinear flutter analyses in point 1 (see Figure 4.6) for both load factors.

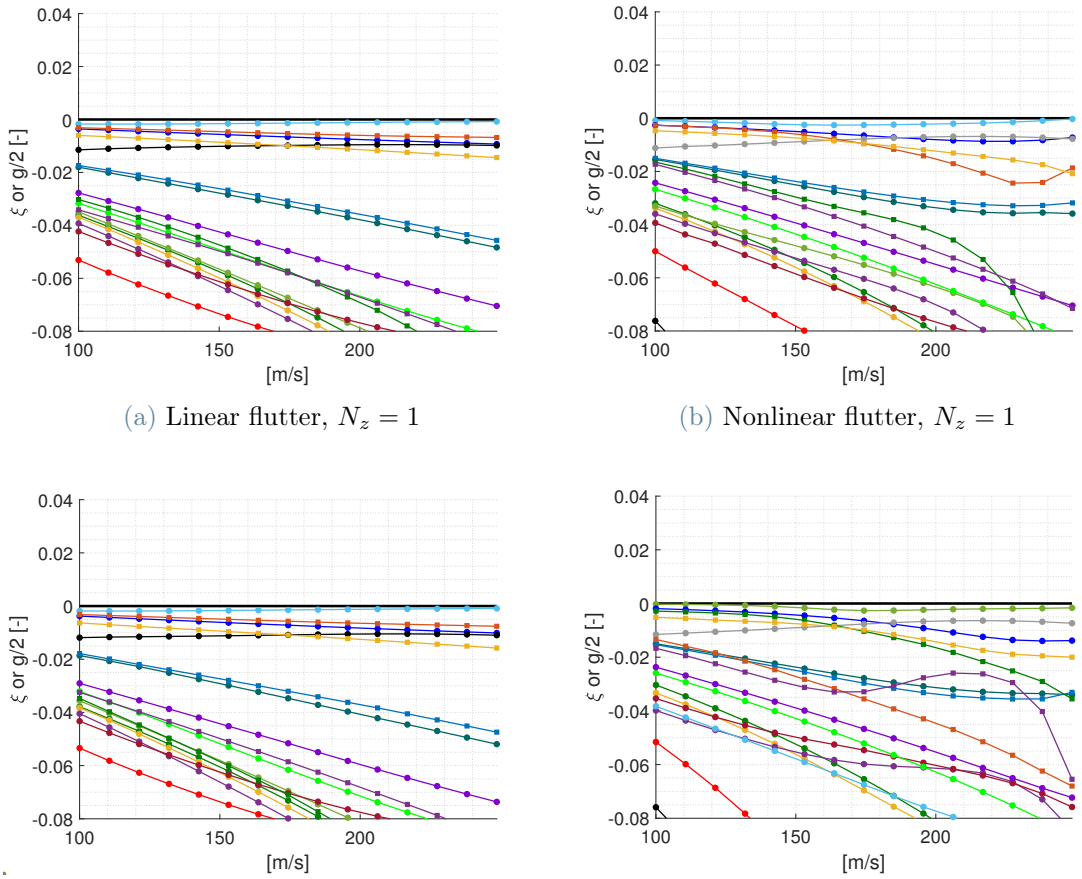

(a) Linear flutter, $N_z = 1$

(b) Nonlinear flutter, $N_z = 1$

(c) Linear flutter, $N_z = 2.5$

(d) Nonlinear flutter, $N_z = 2.5$

Figure 4.8: Flutter results for point 1

As one can notice, the results between the linear and nonlinear analyses at a given load factor change. It is therefore important, if possible, to account for nonlinearities, because the geometrical stiffness matrix generates different modes with respect to the linear ones, which could also lead to aeroelastic behaviors that are not estimated in the linear analyses. For instance, comparing Figures 4.8a and 4.8b, one can notice that for the last velocity (i.e. 1.15VD) the nonlinear results produce a mode which reaches zero damping, while the linear correspondent damping is close to zero but still negative. However, since the

regulations require for a 2% of structural damping, which is not yet introduced in these analyses, the zero damping velocity has not been considered flutter. Another observation that can be pointed out is that considering nonlinear analyses allows to appreciate the difference in the results with changed load factor (i.e. Figures 4.8b and 4.8d). In this case, the increased load factor appears to delay the reaching of zero damping. This feature is lost when considering only linearity.
In any case it can be concluded that, for point 1, no flutter has been detected.
Similar results to the ones presented for point 1 have been obtained also for points 2 and 3, where only the results for $N_z = 1$ are reported in Figures 4.9 and 4.10, to avoid useless repetitions.

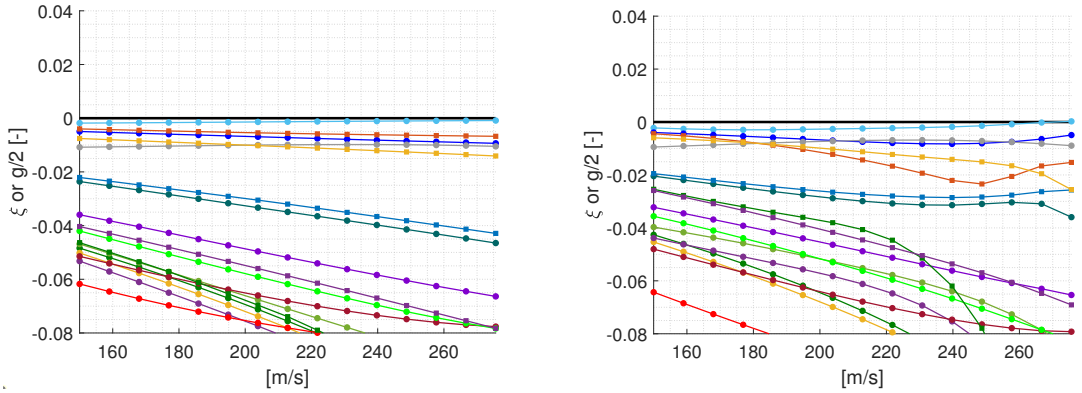

(a) Linear flutter, $N_z = 1$ (b) Nonlinear flutter, $N_z = 1$

Figure 4.9: Flutter results for point 2

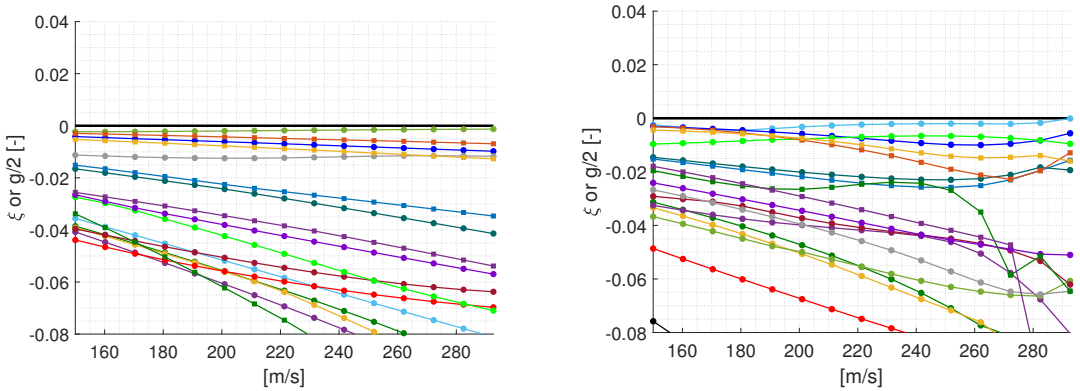

(a) Linear flutter, $N_z = 1$ (b) Nonlinear flutter, $N_z = 1$

Figure 4.10: Flutter results for point 3

As one can notice, in Figure 4.10b some non-smooth mode tracking is present. This is due

to the fact that, for this aircraft, several modes in a relatively small range of frequencies are present, as it was stated discussing Table 2.9, leading to a difficult distinction between very close modes.
Nevertheless, for the investigated points no flutter has been detected.
For what concerns divergence, the dynamic pressure obtained for all the three points is widely outside the flight envelope, as can be seen in Table 4.3, meaning that also divergence is not an issue for the model.

	q_{max} [Pa]	q_{div} [Pa]
Point 1	31118	72771
Point 2	31118	66486
Point 3	25942	51326

Table 4.3: Divergence results

However, as anticipated, only linear divergence has been studied. To have a complete overview of the aeroelastic stability analyses, also nonlinear cases should be adressed, but at the moment it is not possible with NeoCASS.

4.2. Part II: parametric analyses

In this Section, the impact of some parameters on the results is studied. In particular, as anticipated, the parameters chosen are: wing and strut material, mass configuration, strut geometry and wing-strut attachment chordwise position. A comparison of model sizing is given by means of wing and strut weights and normal frequencies. Trim in cruise is then investigated. It is verified whether or not gusts should be included in the sizing process. Finally the effect on flutter and divergence results is presented.

4.2.1. Impact of wing and strut material

The models compared in this Subsection are summarized in Table 4.4. The only difference is the material employed for wing and strut: for the first model, which is the reference model presented before, isotropic material (i.e. Aluminium Alloy AL7075-T6 presented in Table 2.3), while for the second one a composite Carbon Fiber symmetric and balanced (presented in Table 4.5).

	Reference	Composite
Material	AL7075-T6	CFUD $[0/45/-45/90]_s$
Mass configuration	OEW	OEW
Strut geometry	straight	straight
Wing-strut attachment	on EA	on EA

Table 4.4: Compared models: change of wing and strut material

	Value	Unit
$\mathbf{E_{11}}$	135	GPa
$\mathbf{E_{22}}$	10	GPa
$\boldsymbol{\nu_{12}}$	0.3	-
$\boldsymbol{\nu_{21}}$	0.0222	-
$\mathbf{G_{12}}$	5	GPa
$\boldsymbol{\rho}$	1500	$\frac{\text{kg}}{\text{m}^3}$
$\boldsymbol{\sigma_{1T,C}}$	607	MPa
$\boldsymbol{\sigma_{2T,C}}$	45	MPa
$\boldsymbol{\tau_{12}}$	45	MPa
$\mathbf{G_{13}}$	2.8	GPa
$\mathbf{G_{23}}$	2.8	GPa

Table 4.5: CFUD

Sizing

	Reference [kg]	Composite [kg]	Δ%
Half Wing Structural Mass	5976.4	3946.7	34
Half Strut Structural Mass	1796.9	1349.9	25
Total Half Structural Mass	7773.3	5296.6	32

Table 4.6: Structural mass comparison between reference and composite models

During the sizing process described in Figure 2.7, material change has been introduced inside the optimization problem, thanks to the possibility of NeOPT to choose different materials for the components to be optimized. The solution obtained with composite is compared to the one with isotropic material (i.e. reference model), in Table 4.6. Figure 4.11 and Figure 4.12 show the obtained thicknesses for wing and strut of the reference and composite models.

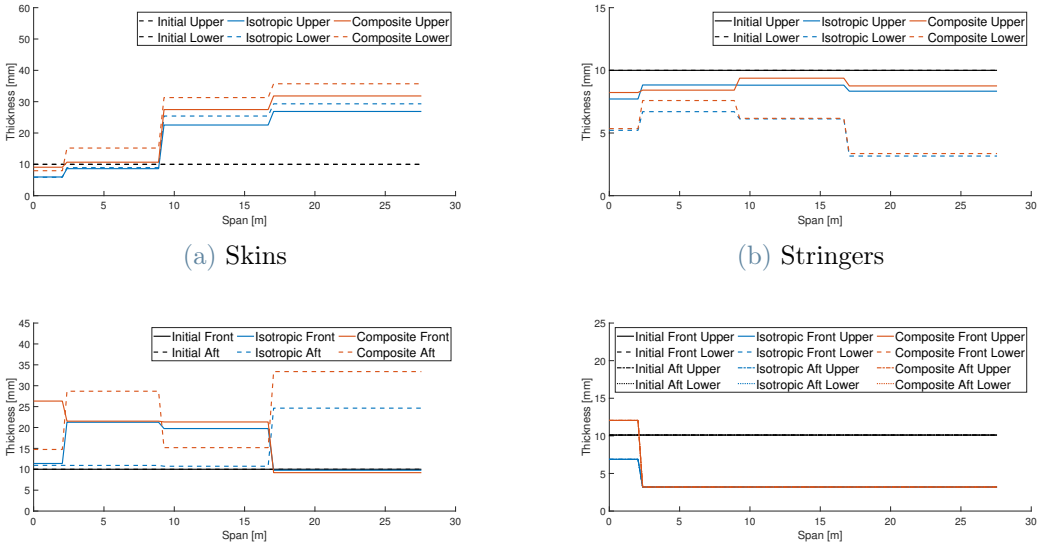

(a) Skins

(b) Stringers

(c) Webs

(d) Sparcaps

Figure 4.11: Wing thicknesses comparison between reference and composite models

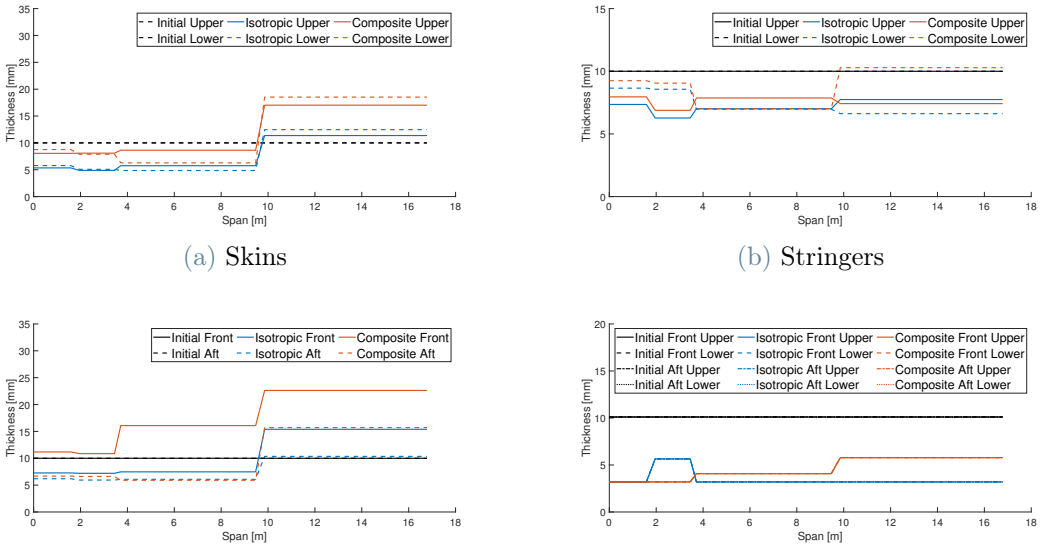

(a) Skins

(b) Stringers

(c) Webs

(d) Sparcaps

Figure 4.12: Strut thicknesses comparison between reference and composite models

Also the stiffnesses are compared, as shown in Figure 4.13.

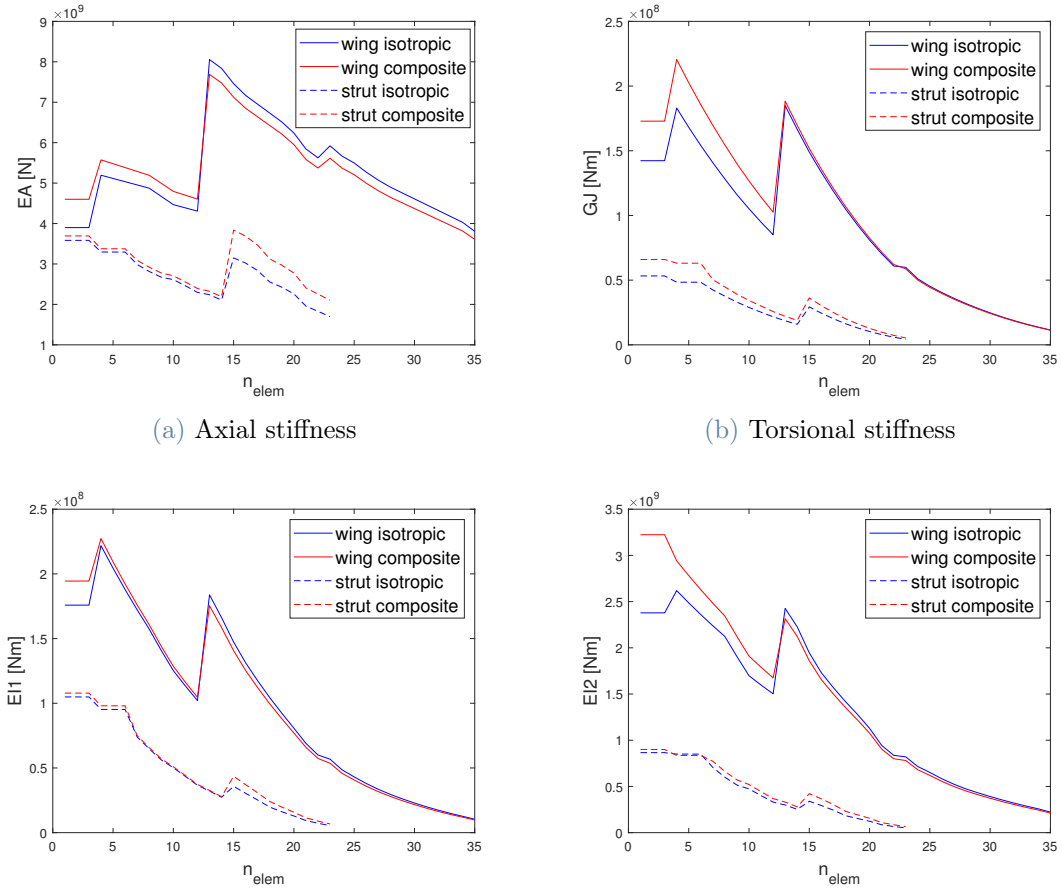

(a) Axial stiffness

(b) Torsional stiffness

(c) Out-of-plane bending stiffness

(d) In-plane bending stiffness

Figure 4.13: Comparison of wing and strut stiffnesses between reference and composite models

Thanks to the high performances of composites, important mass savings are obtained, keeping the stiffnesses more or less unchanged. This leads to an increase in natural frequencies, as reported in Table 4.7.

	Reference [Hz]	Composite [Hz]
Mode 1	1.05	1.25
Mode 2	1.57	1.77
Mode 3	2.24	2.56
Mode 4	2.32	2.61
Mode 5	3.08	3.26

Table 4.7: Natural frequencies comparison between reference and composite models

Trim

The same trim analysis performed for the reference model, has been repeated for the composite one. Figures 4.14 and 4.15 show composite deformed configuration, which is very similar to reference one (presented in Figures 4.1 and 4.2). In order to quantify the differences, Table 4.8 is reported.

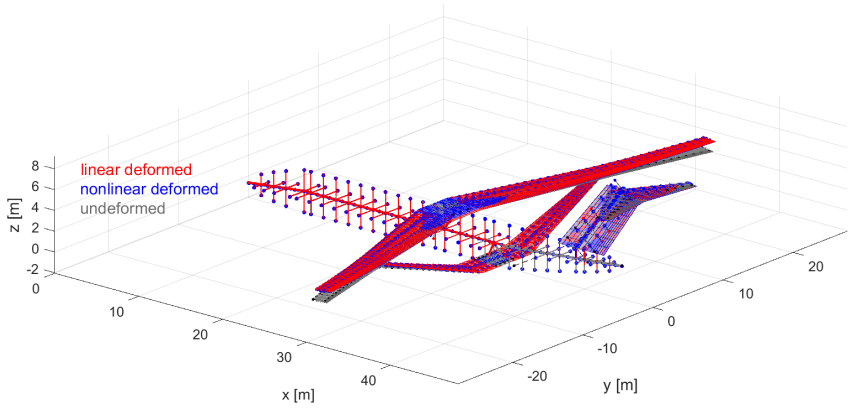

Figure 4.14: Trim in cruise for composite model

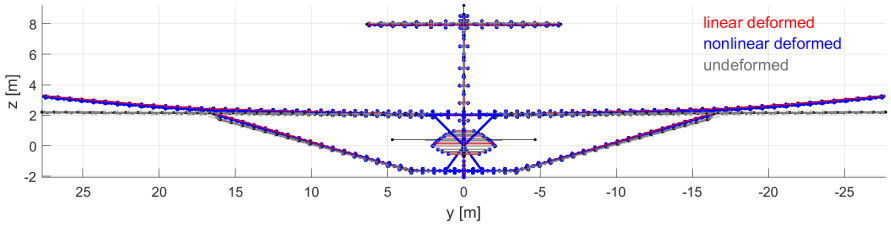

Figure 4.15: Trim in cruise for composite model (front view)

	L Ref	L Comp	$\Delta_L\%$	NL Ref	NL Comp	$\Delta_{NL}\%$
Vertical Displ [m]	1.16	1.05	9.5	1.01	1.00	0.3
Torsion [deg]	−1.75	−1.7	2.8	−1.6	−1.7	6.2

Table 4.8: Wing tip linear (L) vs nonlinear (NL) comparison between reference (Ref) and composite (Comp) models

Gust

The same gust analyses performed for the reference model have been reproposed for the composite one. A comparison of $2D$ plots at wing root and wing-strut attachment sections is reported in Figure 4.16.

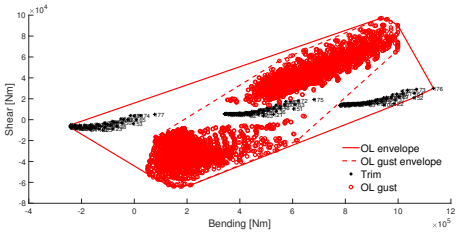

(a) Bending vs Shear (wing root, reference)

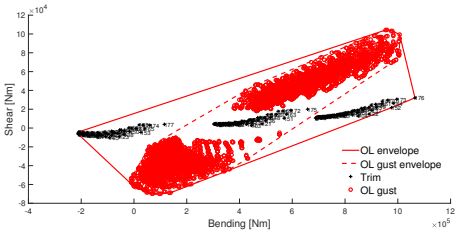

(b) Bending vs Shear (wing root, composite)

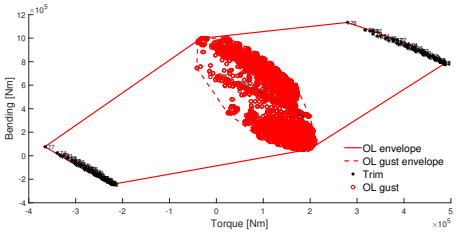

(c) Torque vs Bending (wing root, reference)

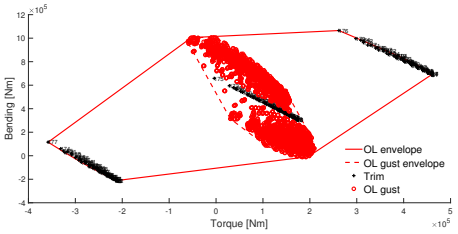

(d) Torque vs Bending (wing root, composite)

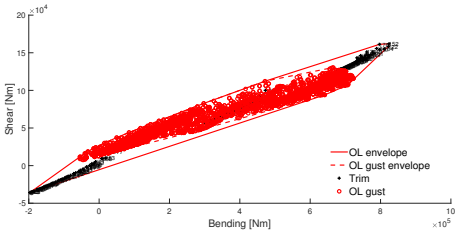

(e) Bending vs Shear (wing-strut attachment, reference)

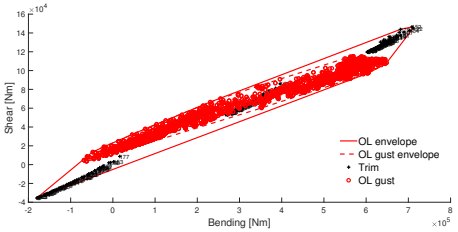

(f) Bending vs Shear (wing-strut attachment, composite)

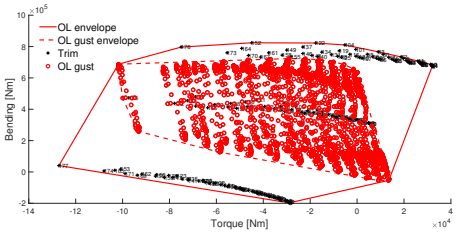

(g) Torque vs Bending (wing-strut attachment, reference)

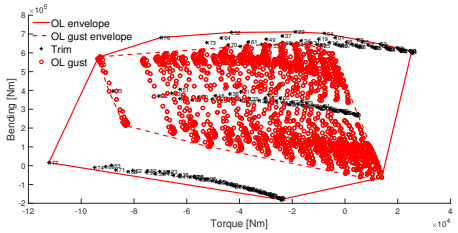

(h) Torque vs Bending (wing-strut attachment, composite)

Figure 4.16: Comparison of wing $2D$ plots with gust between reference and composite models

As one can notice, the results for these sections are very similar. As it was shown for the reference model, also in this case it is possible to analyze maxima and minima envelopes, as reported in Figure 4.17, and check if structural sizing must be updated or is able to sustain the studied gusts.

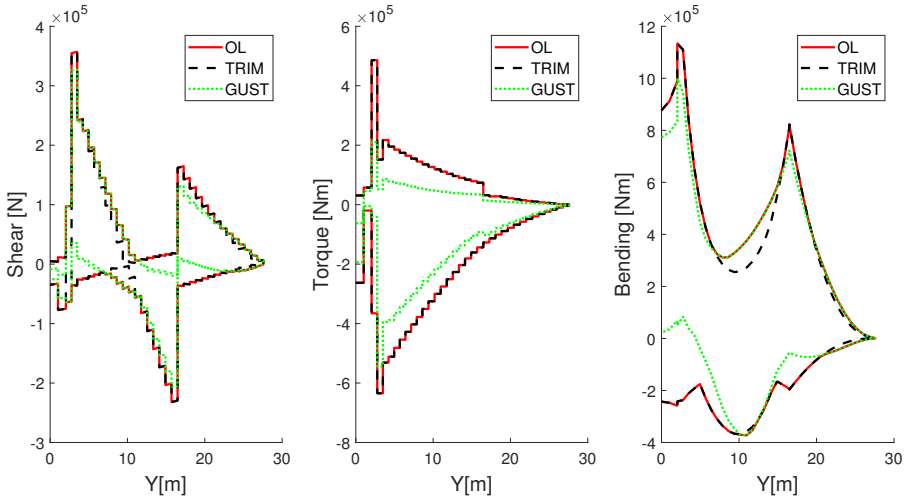

(a) Reference model

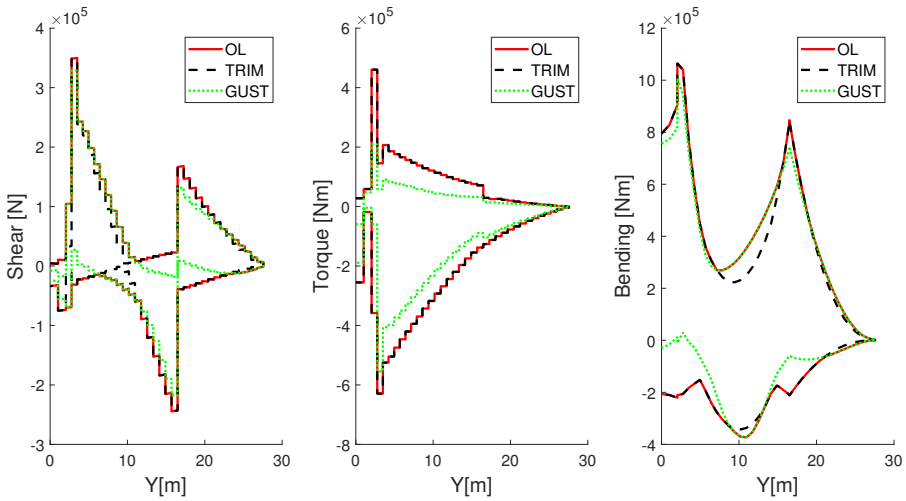

(b) Composite model

Figure 4.17: Comparison of wing maxima and minima spanwise envelopes with and without gust between reference and composite models

Also in case of composite material, as it was for reference model, even if there are some regions where gust loads exceed trim ones, the sized structure is still able to sustain them, hence no sizing update is required.

Divergence and flutter

As it was for trim and gust, also divergence and flutter have been performed following the same path presented for the reference model.
Figure 4.18 shows flutter results for composite model in flight point 1.

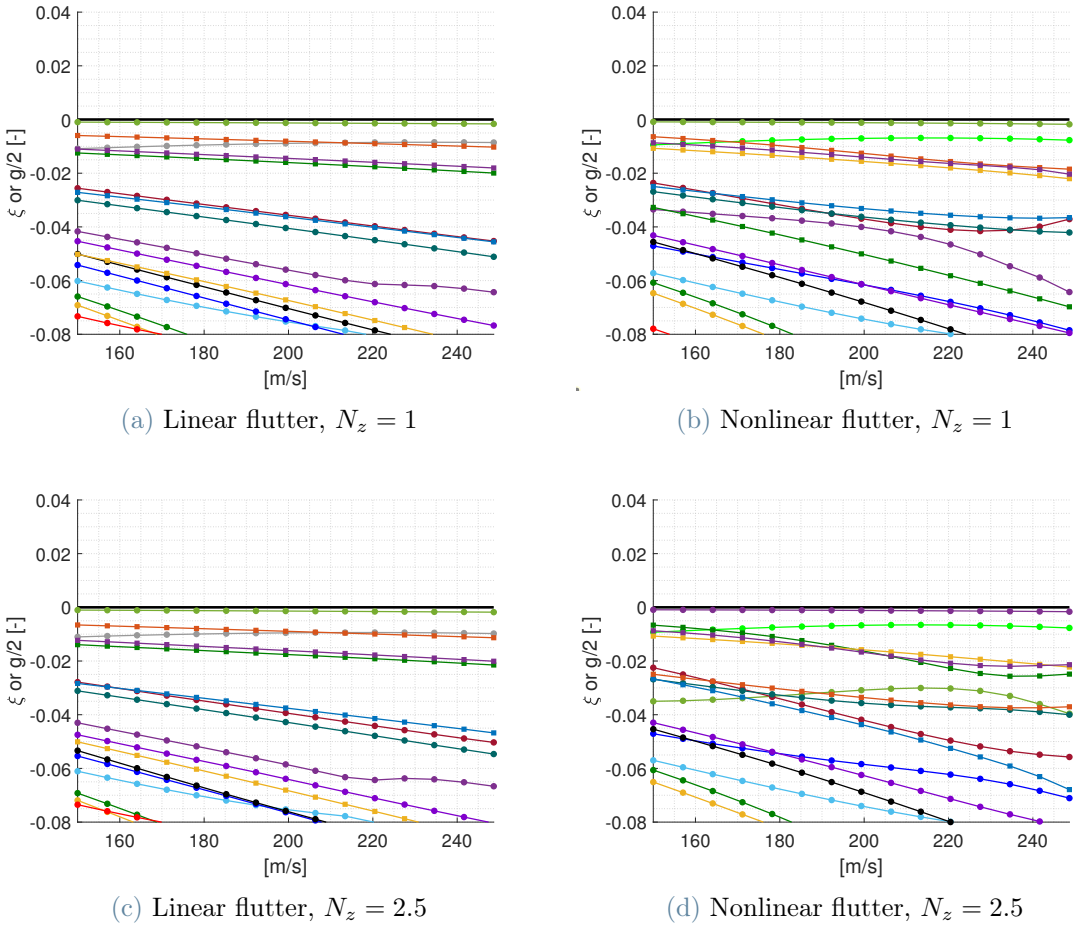

(a) Linear flutter, $N_z = 1$

(b) Nonlinear flutter, $N_z = 1$

(c) Linear flutter, $N_z = 2.5$

(d) Nonlinear flutter, $N_z = 2.5$

Figure 4.18: Flutter results for point 1, composite model

Comparing these results with the reference model ones (Figure 4.8), also in this case the discrepancy between linear and nonlinear analyses at a given load factor, as much as the one between nonlinear analyses with different load factors can be appreciated. However, in case of composite material, for flight point 1 there is no longer the reaching of zero damping inside the studied velocity range. This result is confirmed in Figures 4.19 and 4.20, where nonlinear flutter analyses for points 2 and 3 are reported for both reference and composite models.

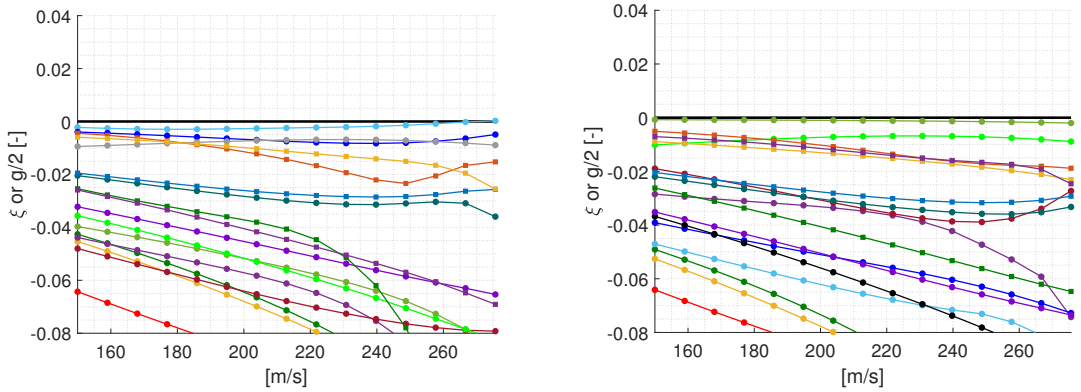

(a) Noninear flutter, $N_z = 1$, reference (b) Nonlinear flutter, $N_z = 1$, composite

Figure 4.19: Comparison of nonlinear flutter results for point 2 between reference and composite models

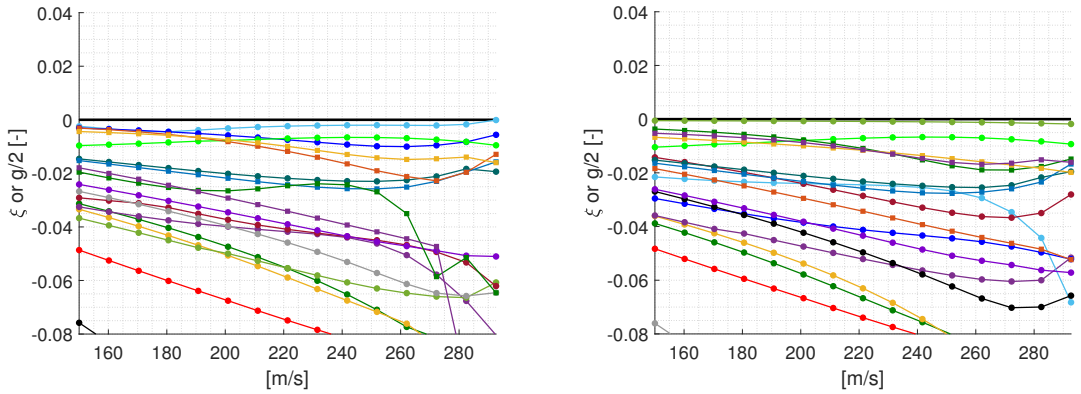

(a) Nonlinear flutter, $N_z = 1$, reference (b) Nonlinear flutter, $N_z = 1$, composite

Figure 4.20: Comparison of nonlinear flutter results for point 3 between reference and composite models

It can be concluded that, also for composite material, for the investigated points no flutter has been detected. Moreover, the presence of composite instead of isotropic material, seems to delay the reaching of zero damping.
The delay effect has been observed also in the divergence analyses, whose results are reported in Table 4.9.

	q_{max} [Pa]	Ref q_{div} [Pa]	Comp q_{div} [Pa]
Point 1	31118	72771	87401
Point 2	31118	66486	79925
Point 3	25942	51326	61927

Table 4.9: Comparison of divergence results between reference (Ref) and composite (Comp) models

4.2.2. Impact of mass configuration

Table 4.10 reports the models analyzed in the present Subsection. While in the previous comparison study the objective was to try to understand how the change of wing and strut material affects the results, now the focus is on mass configuration. Maximum Take-Off Weight (MTOW), Maximum Zero Fuel Weight (MZFW) and Operative Empty Weight (OEW) are considered. Being the employed material composite with lamination sequence of $[0/45/-45/90]_s$, the model with OEW is the one that was named *composite model* in the previous Subsection, as can be noticed comparing the last column of Table 4.4 with the present one.

	Composite MTOW	**Composite MZFW**	**Composite OEW**
Material	CFUD	CFUD	CFUD
Mass configuration	MTOW	MZFW	OEW
Strut geometry	straight	straight	straight
Wing-strut attachment	on EA	on EA	on EA

Table 4.10: Compared models: change of mass configuration

Sizing

As it was for material change, also the different mass configuration was set during the optimization phase of sizing. Table 4.11 compares the obtained wing and strut massess in the three cases. As expected, the highest mass is associated to MTOW while the lowest to OEW.

	Composite MTOW [kg]	Composite MZFW [kg]	Composite OEW [kg]
Half Wing Structural Mass	4541.3	4306.1	3946.7
Half Strut Structural Mass	1879.1	1794.7	1349.9
Total Half Structural Mass	6420.4	6100.8	5296.6

Table 4.11: Structural mass comparison between composite MTOW, MZFW and OEW models

Stiffnesses and modal frequencies are reported in Figure 4.21 and Table 4.12 respectively.

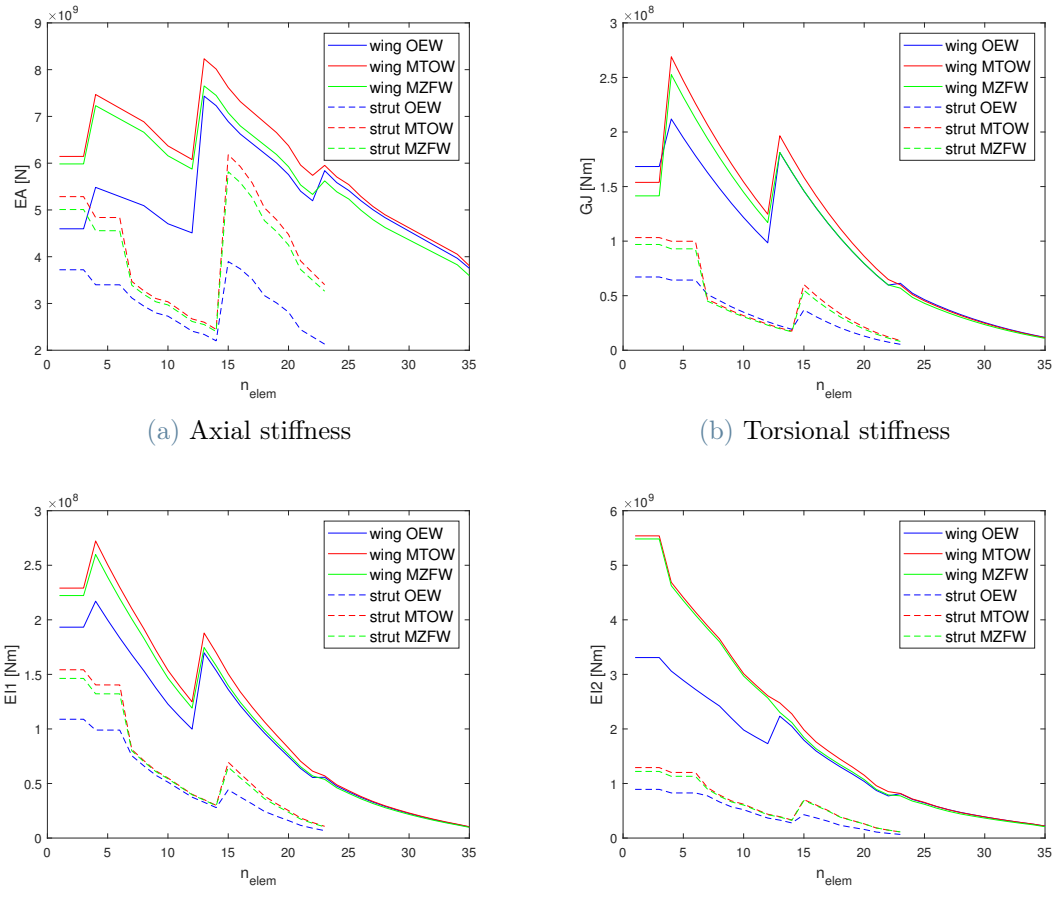

(a) Axial stiffness

(b) Torsional stiffness

(c) Out-of-plane bending stiffness

(d) In-plane bending stiffness

Figure 4.21: Comparison of wing and strut stiffnesses between composite MTOW, MZFW and OEW models

	Composite MTOW [Hz]	Composite MZFW [Hz]	Composite OEW [Hz]
Mode 1	1.31	1.35	1.25
Mode 2	1.72	1.81	1.77
Mode 3	2.5	2.62	2.56
Mode 4	2.52	2.73	2.61
Mode 5	3.11	3.21	3.26

Table 4.12: Natural frequencies comparison between composite MTOW, MZFW and OEW models

Theoretically, an increase in natural frequencies with decreasing weight is expected. However, since also the stiffnesses change between the mass configurations, the presented results are obtained.

Trim

The deformed configurations for trim in cruise are reported in Figure 4.22, where only the front view is shown.
As previously presented, also in this case the differences between linear and nonlinear analyses for the three masses are quantified in Table 4.13.

	L MTOW	L MZFW	L OEW	NL MTOW	NL MZFW	NL OEW
Vertical Displ [m]	1.31	1.25	1.05	1.43	1.39	1.00
Torsion [deg]	−1.82	−1.86	−1.7	−2.12	−2.16	−1.7

Table 4.13: Wing tip linear (L) vs nonlinear (NL) comparison between composite MTOW, MZFW and OEW models

For MTOW and MZFW nonlinear deformations are higher with respect to linear ones, while for OEW the contrary occurs. Moreover, for both linear and nonlinear analyses, the highest wing tip vertical displacement happens for the highest weight (i.e. MTOW).

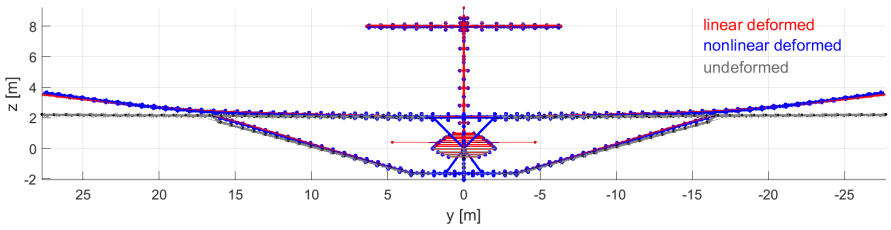

(a) MTOW

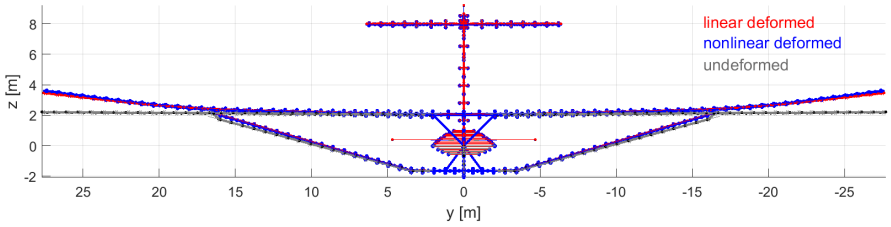

(b) MZFW

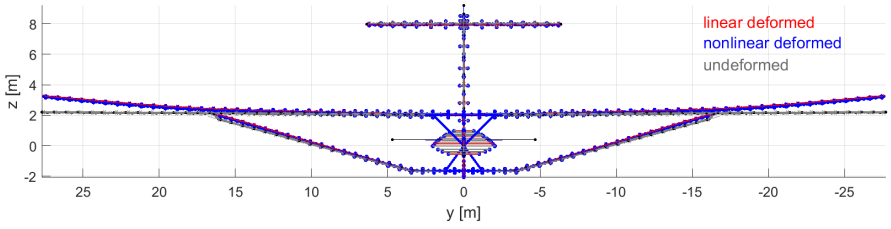

(c) OEW

Figure 4.22: Comparison of trim in cruise between composite MTOW, MZFW and OEW models (front view)

Gust

Only maxima and minima envelopes are reported in Figure 4.23.

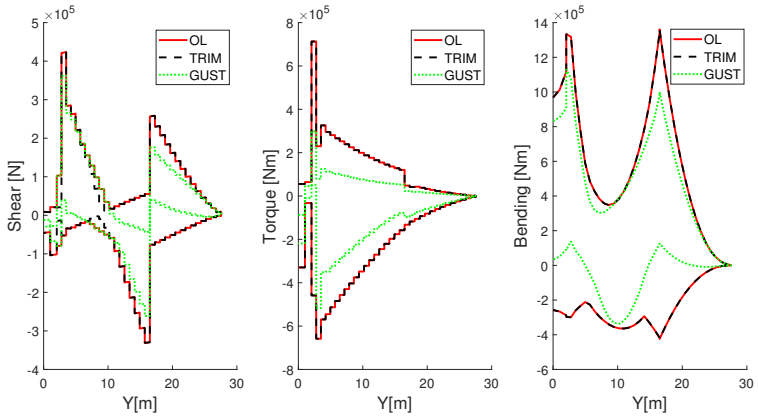

(a) MTOW

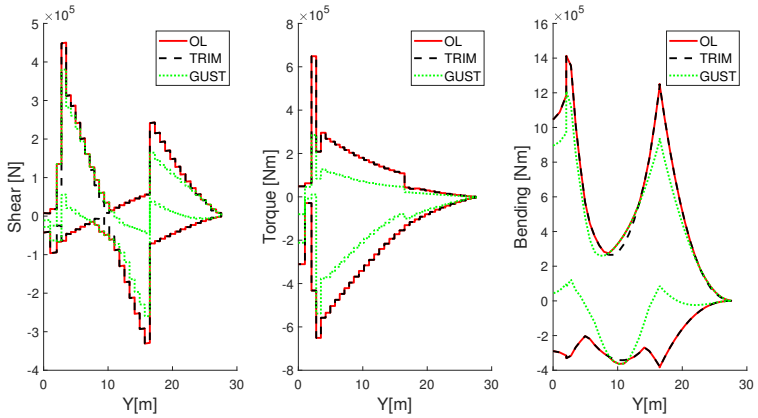

(b) MZFW

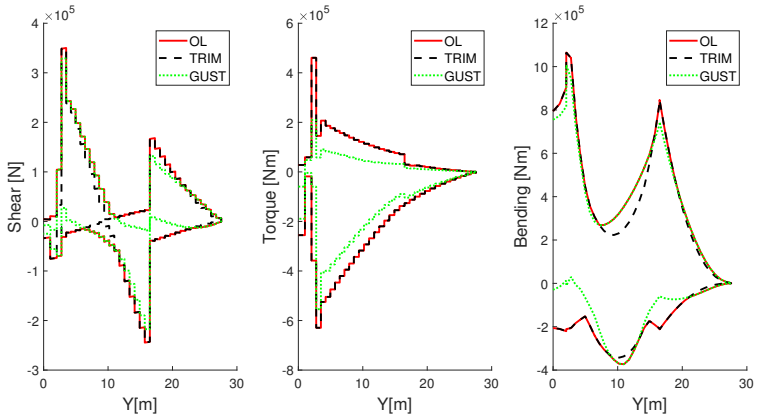

(c) OEW

Figure 4.23: Comparison of wing maxima and minima spanwise envelopes with and without gust between composite MTOW, MZFW and OEW models

Focusing on bending moment, it can be noticed how, by changing mass configurations, the maximum in wing-strut attachment section changes significantly, accordingly to the different deformability already evidenced during trim analysis. Moreover, in case of MTOW, gust envelope is entirely contained inside trim, meaning that there are no wing sections where bending moment maxima and minima are due to gust instead of trim. This is no longer valid for MZFW and OEW, where in the center wing sections the extreme internal actions are caused by gust.
In any case, it has been verified that the sized models are able to sustain all the studied gust loads without presenting buckling nor failure.

Divergence and flutter

Only results concerning nonlinear flutter analysis in point 3 are reported in Figure 4.24.

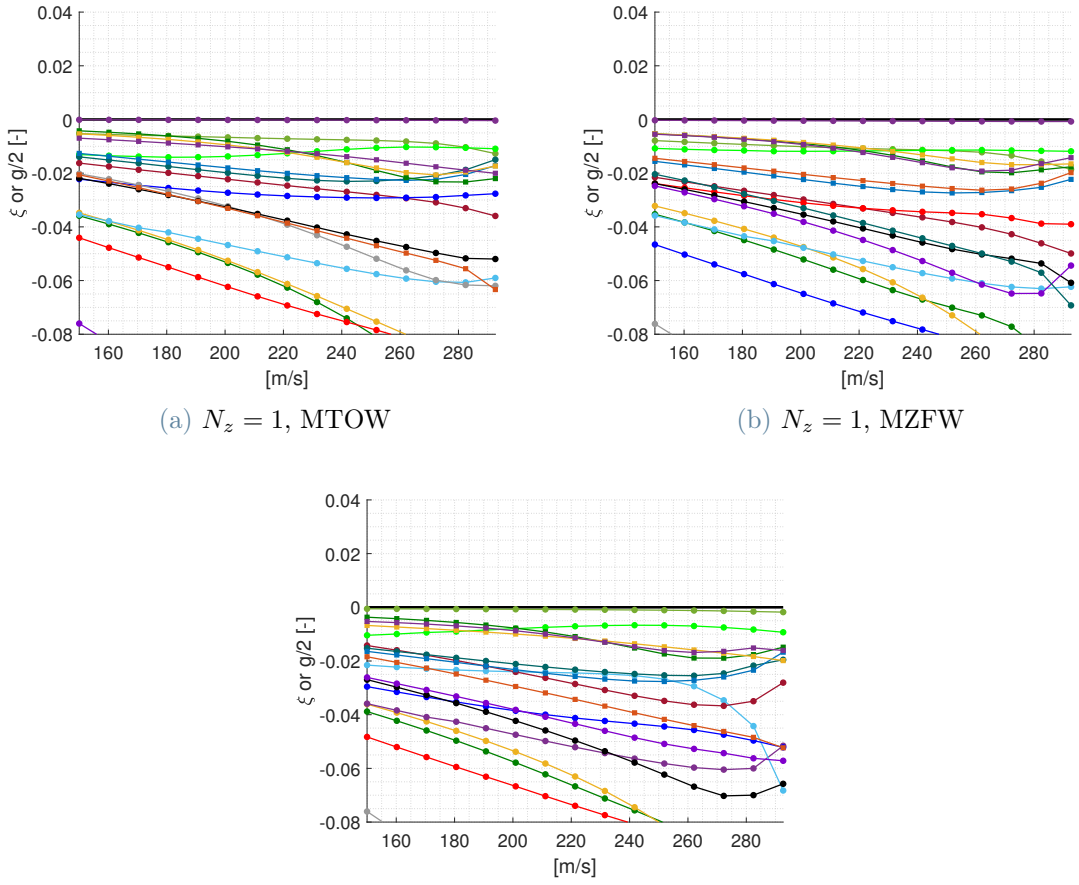

(a) $N_z = 1$, MTOW

(b) $N_z = 1$, MZFW

(c) $N_z = 1$, OEW

Figure 4.24: Comparison of nonlinear flutter results for point 3 between MTOW, MZFW and OEW composite models

For MTOW and MZFW the presence of a mode with nearly constant damping very close to zero can be observed. Also for OEW there is a mode that has a damping very close to zero, but it tends to become more and more negative as velocity increases. Other than that, no big differences are found between the considered mass configurations, for the tested flight point. Indeed, for all three cases, no flutter has been detected.
The effect of mass configuration on divergence dynamic pressure is reported in Table 4.14.

	q_{max} [Pa]	MTOW q_{div} [Pa]	MZFW q_{div} [Pa]	OEW q_{div} [Pa]
Point 1	31118	109080	100145	87401
Point 2	31118	100261	92000	79925
Point 3	25942	78991	72411	61927

Table 4.14: Comparison of divergence results between composite MTOW, MZFW and OEW models

In all the cases the dynamic pressure obtained from the analyses is well beyond the maximum reachable. However it can be observed that the increase of mass seems to have a positive effect on divergence phenomenon, because, as it was presented in Figure 4.21, the higher the payload weight, the higher the structural stiffness.

4.2.3. Impact of strut geometry

Recalling that this work focuses on Strut-Braced Wing (SBW), it must be pointed out that the presence of strut generates some aerodynamic uncertainties due to the interaction with wing. Pure aerodynamic studies are out of the scope of this thesis. However, in literature, some effort has been spent to understand the aerodynamics of such configurations. The drag component generated between wing and strut is named interfence drag, and, e.g. in [12] and in [20], it was concluded that increasing the offset between wing and strut can have a beneficial effect on it. This offset has been introduced by means of a change in strut geometry. Even if the methods used in the analyses presented in Chapter 3 do not account for interference drag, it can be interesting to check what happens to the results because of this change. The compared models are summarized in Table 4.15, where the composite straight model is the same named *composite model* in Subsection 4.2.1 and *composite OEW model* in Subsection 4.2.2.

	Composite straight	Composite curved
Material	CFUD	CFUD
Mass configuration	OEW	OEW
Strut geometry	straight	curved
Wing-strut attachment	on EA	on EA

Table 4.15: Compared models: change of strut geometry

To clarify which geometrical changes have been produced, Figure 4.25 shows the two models under comparison.

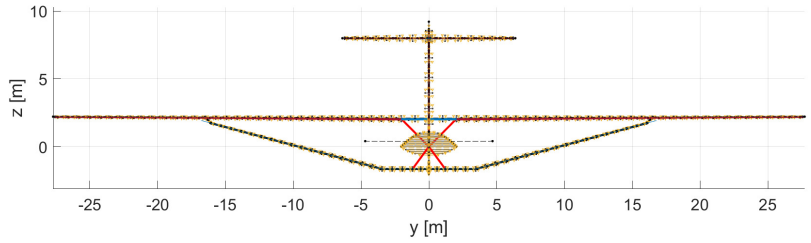

(a) Straight

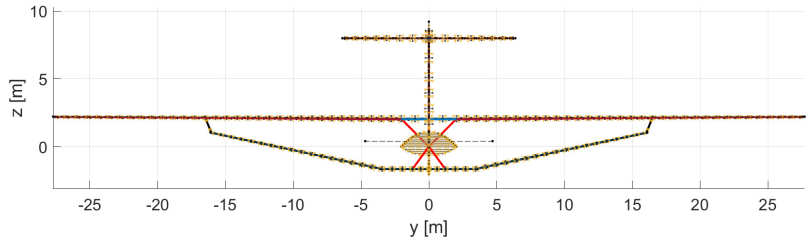

(b) Curved

Figure 4.25: Compared models: change of strut geometry (front view)

Sizing

Also in this case, as it was for change of material and mass configuration, the strut geometry has been re-assigned before launching the optimization problem. Table 4.16 shows the obtained results.

	Composite straight [kg]	Composite curved [kg]	Δ%
Half Wing Structural Mass	3946.7	4006.9	1.5
Half Strut Structural Mass	1349.9	2098.8	35.7
Total Half Structural Mass	5296.6	6105.7	13.25

Table 4.16: Structural mass comparison between composite straight and curved models

For the curved model, strut mass is higher. In order to understand this result, one can look at the estimated stiffnesses.

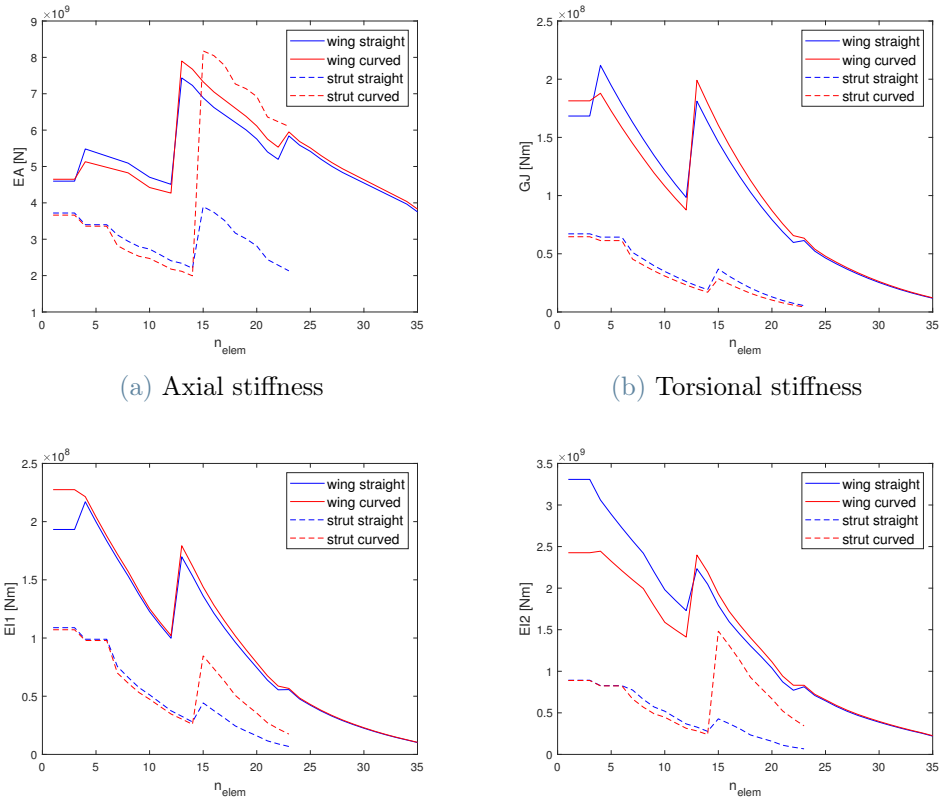

(a) Axial stiffness

(b) Torsional stiffness

(c) Out-of-plane bending stiffness

(d) In-plane bending stiffness

Figure 4.26: Comparison of wing and strut stiffnesses between composite straight and curved models

As visible in Figure 4.26, curved strut tip portion has been oversized with respect to the straight case. This leads to an increase in mass. On the contrary, wing can be considered more or less unchanged.
Table 4.17 reports the natural frequencies. Consistently with what just stated, due to the increase in mass, the curved model natural frequencies are lower with respect to the straight ones.

	Composite straight [Hz]	Composite curved [Hz]
Mode 1	1.25	1.13
Mode 2	1.77	1.74
Mode 3	2.56	2.49
Mode 4	2.61	2.50
Mode 5	3.26	2.98

Table 4.17: Natural frequencies comparison between composite straight and curved models

Trim

Figure 4.27 shows the deformed configurations for trim in cruise.
The numerical differences are reported in Table 4.18.

	L straight	**L curved**	$\Delta_L\%$	**NL straight**	**NL curved**	$\Delta_{NL}\%$
Vertical Displ [m]	1.05	1.32	20.4	1.00	1.25	20
Torsion [deg]	−1.7	−1.71	0.6	−1.7	−1.73	1.7

Table 4.18: Wing tip linear (L) vs nonlinear (NL) comparison between composite straight and curved models

The curved model results show a higher deformation with respect to the straight one. For both models, nonlinear vertical displacement is lower than the linear one. Torsional rotations are very similar for all the analyses.

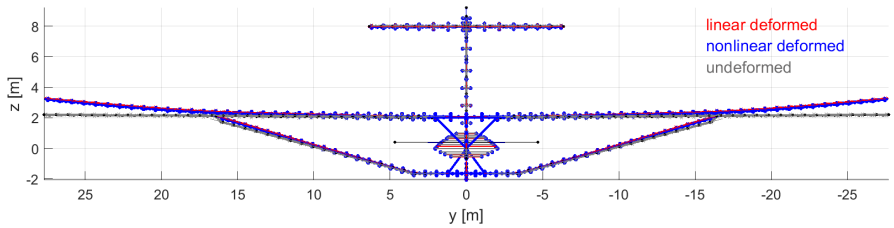

(a) Straight

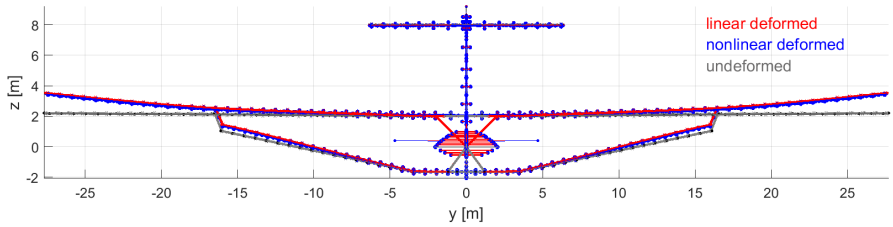

(b) Curved

Figure 4.27: Comparison of trim in cruise between composite straight and curved models (front view)

Gust

The spanwise wing internal actions envelopes are reported in Figure 4.28. The force that most changes between the compared models is bending. In particular, wing root bending moment maximum results to be higher for the curved model. The same is valid also for the minimum, meaning that for this model the largest $2D$ plots are obtained. For both the compared cases, in wing root and wing-strut attachment sections, trim generates the most critical loads. On the contrary, in wing central portion, gusts cause possibly dangerous forces. However, it has been verified that the sized structure is able to sustain such loads. Hence, as it happened for the previous discussed models, no re-sizing has been produced.

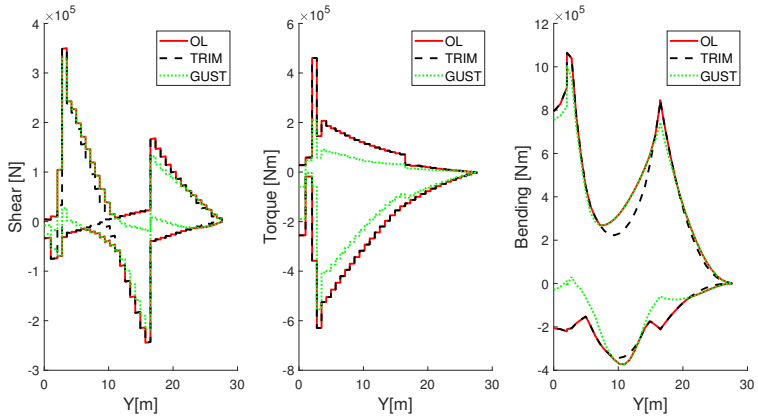

(a) Straight

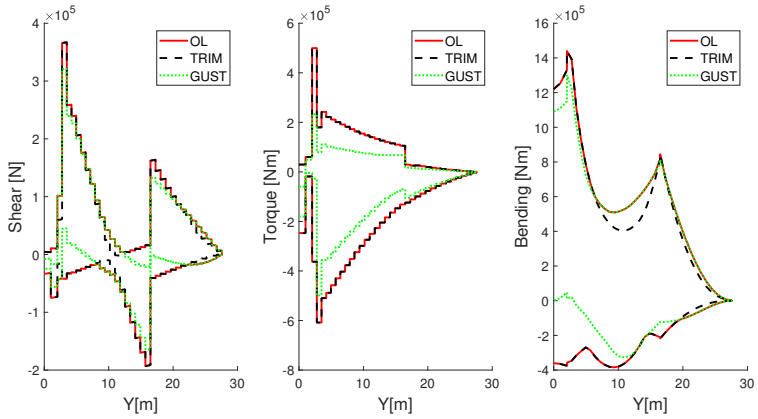

(b) Curved

Figure 4.28: Comparison of wing maxima and minima spanwise envelopes with and without gust between composite straight and curved models

Divergence and flutter

Figure 4.29 shows nonlinear flutter results for the corner point, i.e. point 3 (Figure 4.6). For the curved case, some irregular mode trackings are reported. The reason for this phenomenon has already been discussed and is numerical, therefore it does not represent an issue. Other than that, it can be observed that both the models present a mode that is very close to zero damping, as it was also highlighted for previous cases. The difference is in the tendency of such mode to either reach or not positive damping. Actually, in both cases this situation does not occur, but the curved model seems to go in this direction, while for the straight one the damping becomes more and more negative as velocity increases. Therefore, the presence of an increased offset between wing and strut, which translates in a geometrical change, seems to have a negative effect on flutter.

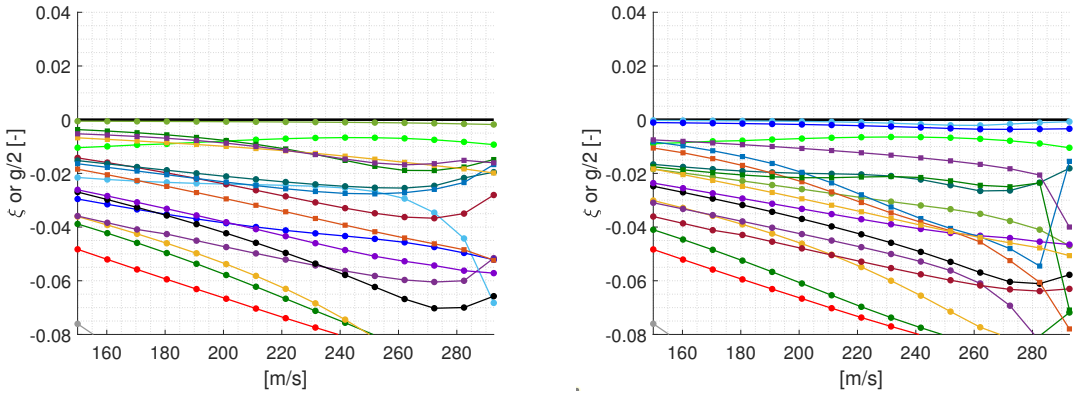

(a) $N_z = 1$, Straight (b) $N_z = 1$, Curved

Figure 4.29: Comparison of nonlinear flutter results for point 3 between composite straight and curved models

Table 4.19 shows linear divergence solutions. The results are similar, meaning that the effect of curved strut does not seem to particularly affect this type of analysis, at least in the considered flight points. However, it must be considered that aerodynamics is modeled through DLM and interference drag is not captured.

	q_{max} [Pa]	Straight q_{div} [Pa]	Curved q_{div} [Pa]
Point 1	31118	87401	89191
Point 2	31118	79925	81150
Point 3	25942	61927	61694

Table 4.19: Comparison of divergence results between composite straight and curved models

4.2.4. Impact of wing-strut attachment chordwise position

In [26], some studies were conducted regarding the position of wing-strut chordwise attachment. Since aircrafts with high Aspect Ratio (AR) are characterized by a smaller wingbox with respect to the conventional configurations, it can be difficult to correctly estimate the structural stiffnesses. In particular, as it was also discussed in Chapter 1, some attention must be focused on the torsional one.

In this context, changing the chordwise position of wing-strut attachment can be bene-

ficial, because an offset with respect to wing EA is introduced along with an associated torsional moment that is accounted for during sizing. Of course, in order to exploit this feature, the software used to produce the model must allow some freedom on the connection between different components.
Since NeoCASS, which is the tool used in the present work, produces a stick model, the aforementioned freedom is not present and the strut is automatically connected on wing EA. As stated in Chapter 2, the torsional stiffness issue was encountered and solved by means of NeCASS optimizer. At this stage no chordwise offset was introduced.
Thanks to NeOPT flexibility, it is however possible to adjust the geometry as desired, and size the updated model. This is the path followed in the present Subsection, where the model changes concern wing-strut attachment chordwise position, to mainly check how they impact on sizing. Table 4.20 summarizes the compared models.

	Composite Front	**Composite EA**	**Composite Rear**
Material	CFUD	CFUD	CFUD
Mass configuration	OEW	OEW	OEW
Strut geometry	straight	straight	straight
Wing-strut attachment	on front spar	on EA	on rear spar

Table 4.20: Compared models: change of wing-strut attachment chordwise position

The middle column reports the same model previously named *composite model* (see Subsection 4.2.1), *composite OEW model* (see Subsection 4.2.2), *composite straight model* (see Subsection 4.2.3).
To clarify the concept, Figure 4.30 shows the different strut positions. In order to change the wing-strut chordwise attachment, the entire strut has been translated along the fuselage axis.

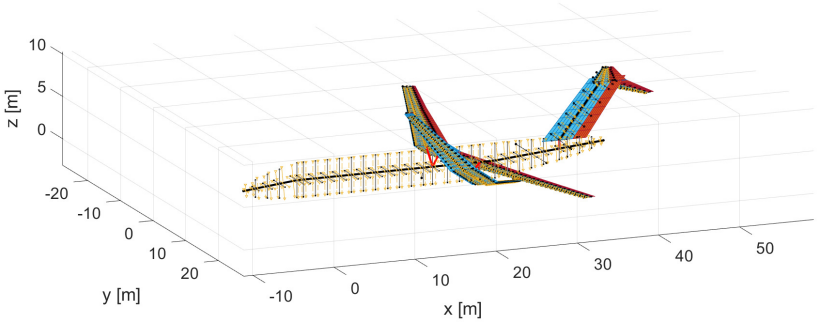

(a) Front

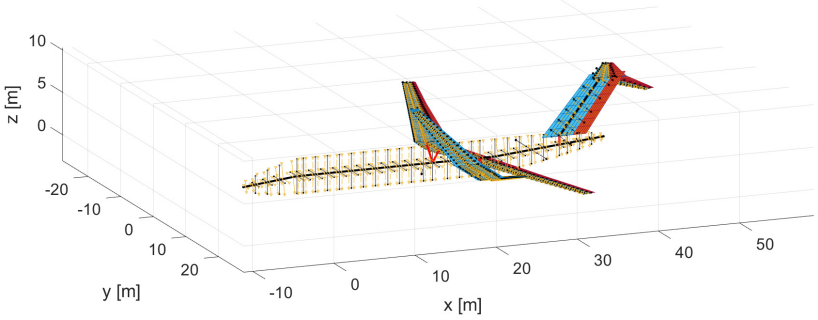

(b) EA

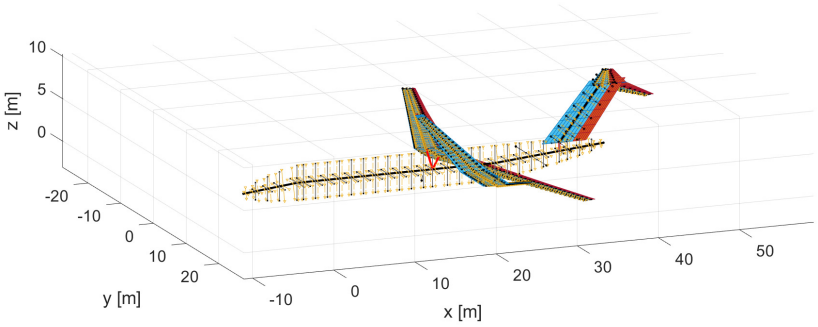

(c) Rear

Figure 4.30: Compared models: change of wing-strut attachment chordwise position

Sizing

Table 4.21 shows the obtained masses for the different strut chordwise position.

	Composite Front [kg]	Composite EA [kg]	Composite Rear [kg]
Half Wing Structural Mass	4233.4	3946.7	3638.2
Half Strut Structural Mass	1307.9	1349.9	1425.6
Total Half Structural Mass	5541.3	5296.6	5063.8

Table 4.21: Structural mass comparison between composite front, EA and rear models

When the strut is attached at the front spar, wing structural mass increases while strut structural mass decreases with respect to the configuration at the EA. On the contrary, when the strut is translated at the rear spar, wing decreases and strut increases. Globally, the lighter configuration is the last one.
Figure 4.31 shows the different stiffnesses, while natural frequencies are compared in Table 4.22. In particular, the effect of the attachment position on torsional stiffness can be appreciated looking at Figure 4.31b.

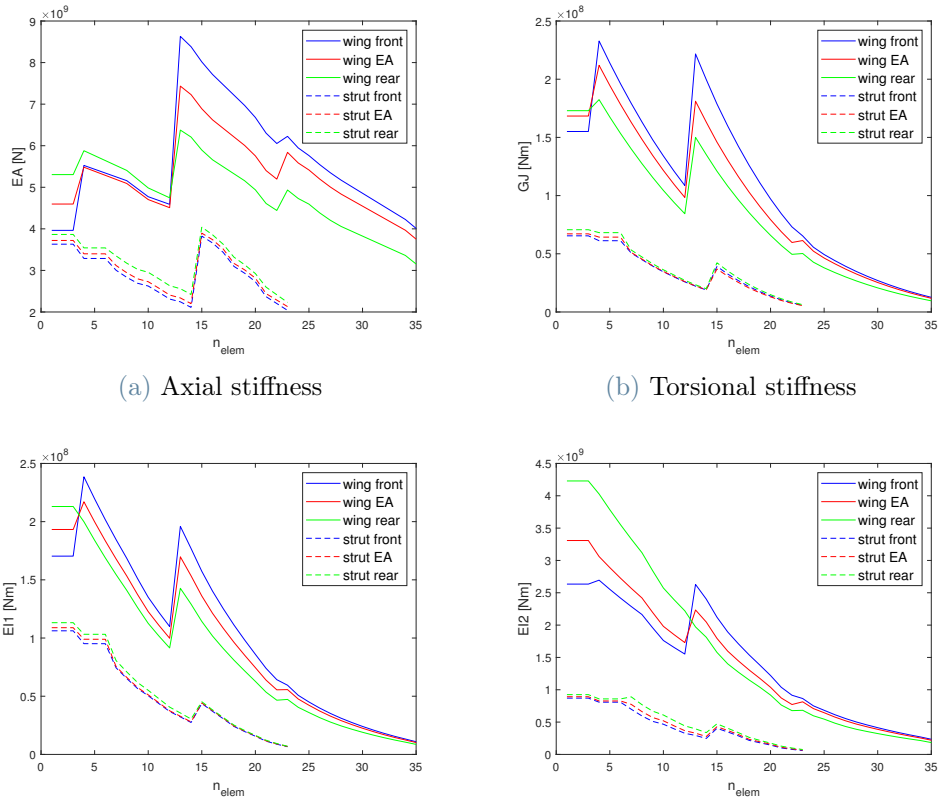

(a) Axial stiffness

(b) Torsional stiffness

(c) Out-of-plane bending stiffness

(d) In-plane bending stiffness

Figure 4.31: Comparison of wing and strut stiffnesses between composite front, EA and rear models

	Composite Front [Hz]	Composite EA [Hz]	Composite Rear [Hz]
Mode 1	1.28	1.25	1.24
Mode 2	1.81	1.77	1.72
Mode 3	2.53	2.56	2.61
Mode 4	2.58	2.61	2.65
Mode 5	3.21	3.26	3.37

Table 4.22: Natural frequencies comparison between composite front, EA and rear models

Trim

Figure 4.32 presents the deformed configurations. As one can notice, the wing-strut attachment chordwise position clearly influences the deflection. The numerical results are collected in Table 4.23.

	L Front	L EA	L Rear	NL Front	NL EA	NL Rear
Vertical Displ [m]	0.91	1.05	1.28	0.83	1.00	1.43
Torsion [deg]	−2.17	−1.7	−1.12	−2.09	−1.7	−1.33

Table 4.23: Wing tip linear (L) vs nonlinear (NL) comparison between composite front, EA and rear models

As one can notice, both wing tip vertical displacement and torsional rotation increase with strut translation along the rear fuselage. Moreover, for the front and EA models, the linear results are higher than the nonlinear ones, while for the rear model the contrary is valid.
Before proceeding, a comment is needed. The reported trim is studied in cruise. However, during the present work, another trim, whose aim has been intended to verify the model, was mentioned: the dive one (Subsection 2.2.1). Even if the results concerning this latter trim were not reported in the present Chapter, it has been evaluated for all the mentioned models, in order to check if they work properly. In the case of composite rear model, trim in dive produced the same problematic results that have been mentioned in Chapter 2 for ONERA model (Figures 2.4 and 2.5). The reason for this behavior, i.e. wing tip bending downwards, must be searched in the balance between aerodynamic loads and weights.

Indeed, if the strut weights enough and the aircraft attitude is such that not sufficient lift is generated, there is not adequate vertical force to counteract the negative jump due to strut weight. This means that tip wing portion is pulled downward. Since the rear composite model hasn't passed the verification test, it is not reported in gust, divergence and flutter results.

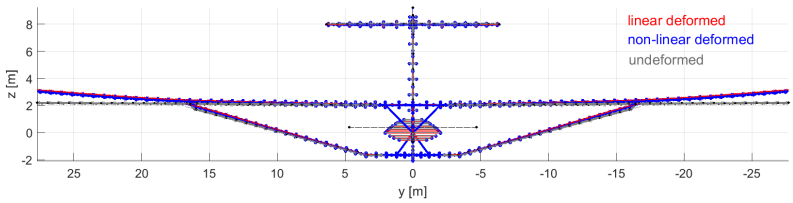

(a) Front

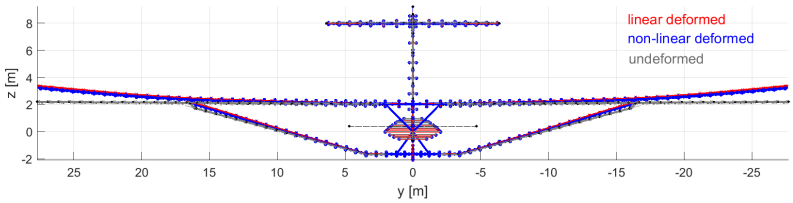

(b) EA

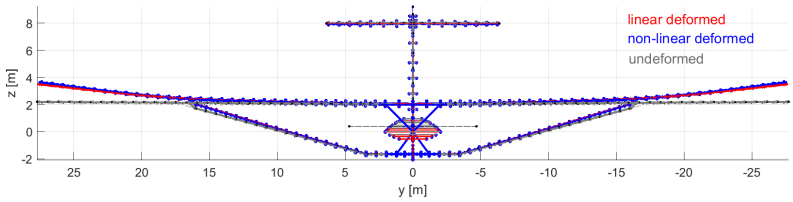

(c) Rear

Figure 4.32: Comparison of trim in cruise between composite front, EA and rear models (front view)

Gust

Figure 4.33 shows the envelopes of maxima and minima for front and EA models.

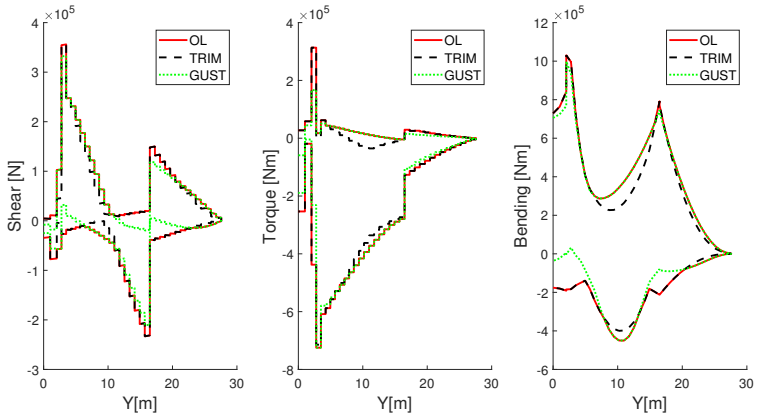

(a) Front

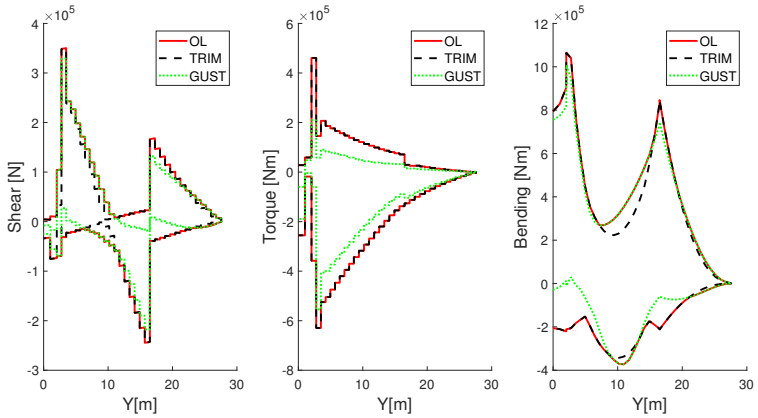

(b) EA

Figure 4.33: Comparison of wing maxima and minima spanwise envelopes with and without gust between composite front and EA models

In this comparison the focus is put on the torsional moment. Indeed, bending moment is very similar between the two models. The same is valid also for shear. While torque differs. In particular, looking at the maximum torsional moment envelope, in wing central region the gust dominates. This discrepancy can be explained considering the wing-strut attachment chordwise position, which indeed generates a different torsional distribution with respect to the one obtained for EA. In any case, also for these models it has been verified that gust does not produce sizing loads.

Divergence and flutter

Figure 4.34 compares the nonlinear flutter results computed in the corner point.

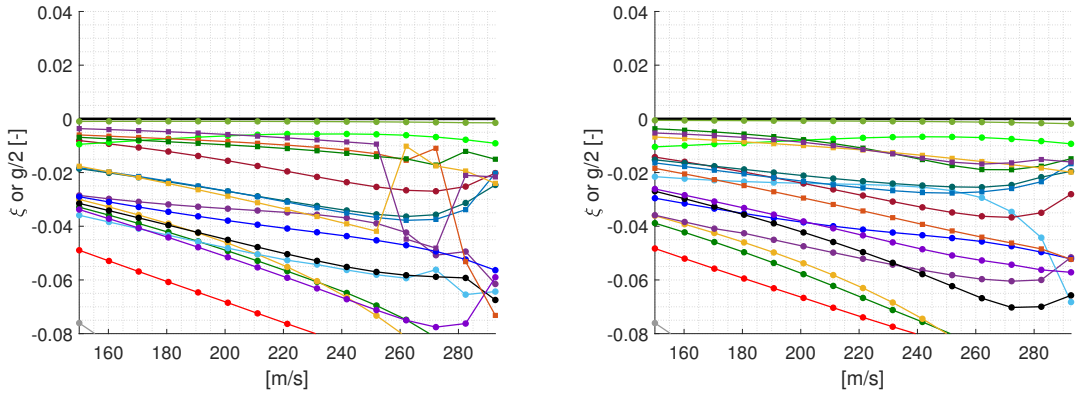

(a) $N_z = 1$, Front (b) $N_z = 1$, EA

Figure 4.34: Comparison of nonlinear flutter results for point 3 between composite front and EA models

As previously discussed, the irregular mode tracking is not an issue. Ignoring this, the obtained results are very similar, especially in the behavior of the mode with damping close to zero. This means that if the strut is translated forward, it keeps the same flutter characteristics as if it is attached at the EA.
The wing-strut attachment on front spar seems to have a beneficial effect on divergence. Also in this case (linear) divergence does not occur inside the flight envelope.

	q_{max} [Pa]	Front q_{div} [Pa]	EA q_{div} [Pa]
Point 1	31118	92721	87401
Point 2	31118	84617	79925
Point 3	25942	64539	61927

Table 4.24: Comparison of divergence results between composite front and EA models

Conclusions and future developments

By now, climate crisis can no longer be ignored. If from one side is natural to ask everyone to do their best for a more sustainable everyday life, it must be admitted that the highest changes need the participation of politics and industry. Aviation is of course part of the game. Indeed, in the last decades several work has been done to create greener aircrafts, improving aerodynamics e.g. acting on profile designs, material expanding composite studies, propulsion by means of efficient engines and employing advanced control laws. Unfortunately, all these interventions, which put together seem huge, do not provide the boost needed nowadays to reach the ambitious objective for Europe to be the first climate-neutral continent by the year 2050 [34]. A change of perspective is required.
Different EU ventures have been started in this context, one of which is part of Clean Sky 2 project and is named Ultra-High Aspect Ratio Wing Advanced Research and Designs (U-HARWARD). One of the objectives of the project was to study the unconventional Strut-Braced Wing (SBW) configuration, which is characterized by a high AR wing sustained by a strut, where the AR helps to reduce the induced drag while the strut mitigates the effect of increasing weight, alleviating wing root bending moment. Some work concerning the SBW has been done by ONERA and ISAE-SUPAERO, who produced an aeroelastic model described in [31]. This can be considered as the starting point of the present work.

After having contextualized the SBW idea and history, a Chapter was dedicated to the aeroelastic model generation. In particular, some important differences between the model studied in this work and the one of ONERA have been highlighted. The most significant discrepancy is in how the wing-strut attachment has been modeled. ONERA followed the idea of exploiting a sleeve that allows the strut to be inactive under compression (i.e. for negative lift). This concept, which was firstly proposed by NASA in the 1990s, was introduced to avoid strut buckling. Indeed, if the strut could experience buckling, this condition would become the driver of its sizing, leading to an increase in weight that could cancel the benefits of reduced induced drag. However, since no dedicated studies were conducted on this connecting mechanism, it is for the moment a non-realistic solution.

Therefore, in the present thesis this assumption was not considered, and the attachment between wing and strut has been modeled through hinges. This of course means that the strut must be able to sustain also compressive loads, hence a higher weight with respect to the ONERA idea is obtained.
The sizing obtained on ONERA geometry, using NeoCASS, produced an underestimation of wing torsional stiffness. For this reason, NeOPT has been exploited requiring a certain amount of aileron efficiency as constraint, which has the effect of increasing the desired stiffness. Once optimized, a trim in dive has been computed for the model. The unexpected result of wing bending downward has been obtained. This was due to the fact that a very small strut has been modeled, but, being it a lifting surface, aerodynamics loads this very flexible component, which, in turns, tends to bend a lot, pulling the wing behind itself. A possible solution was to re-design the strut such that it became much less flexible. Important changes have been made, in particular the wetted area was significantly increased, because the chord was. A modal analysis on the resulted model was computed and a comparison between Classical Tube and Wing (CTW) and SBW was reported as well, in order to appreciate the alleviation of wing root bending moment, while estimating the structural weights.

The typical aeroelastic analyses have been briefly discussed and the importance of considering, when possible, also nonlinear contributions due to the reached large displacements for such flexible structures has been highlighted. The related results have been reported in the dedicated Chapter. In particular, this was divided in two parts.
In the first one, the analyses for the model just discussed have been reported. Linear and nonlinear trim were studied in cruise condition. The results differ of a limited amount. Linear gust was computed and it was verified that no critical loads have been found, meaning that the sizing did not need to be recomputed. Flutter and divergence were studied in the same flight points. In particular, for each condition, two analyses were computed changing the load factor, to see which was its effect on nonlinear results. Some mode with zero damping has been detected, but since the structural damping was not included, it was not considered flutter. Under this condition, indeed, flutter is identified if a mode damping reaches 0.02. However, thanks to the possibility of comparing linear and nonlinear results, it was possible to appreciate the differences between the two approaches. Moreover, increasing the load factor resulted to have a beneficial effect on flutter behavior, delaying the reaching of zero damping. Divergence was studied only linearly and happened widely outside the flight envelope.
In the second part, a set of parametric analyses were conducted. The effect of some model changes on the results (i.e. sizing, linear and nonlinear trim in cruise, linear gust, linear

and nonlinear flutter, linear divergence) was studied. Firstly, the employment of a composite laminate for wing and strut was compared to the one with isotropic Aluminium alloy. Lighter wing and strut were obtained, as expected, thanks to composite characteristics. The differences in nonlinear trim in cruise and linear gust were pretty limited. Composite material seems to have a beneficial impact on flutter. Indeed, if for isotropic model a mode with zero damping was found (but again, it was not considered flutter because of the lack of structural damping), for composite model this occurrence does not verify. Actually, the mode with damping close to zero tends to reach more and more negative values as velocity increases. The benefit of composites reflects also on divergence solution. Then, the effect of mass configuration was adressed. In particular, Maximum Take-Off Weight (MTOW), Maximum Zero Fuel Weight (MZFW) and Operative Empty Weight (OEW) were compared. From sizing, the heaviest structural weight was obtained for MTOW and the lightest for OEW, as expected. The deflection of trim in cruise is smaller for OEW, both for linear and nonlinear analyses. For linear gusts, different enevelopes have been obtained but no re-sizing was needed. Flutter results were very similar for MTOW and MZFW, but in general also for OEW no flutter has been detected. The mass configuration has an effect on divergence results. In particular, the higher the weight, the higher the dynamic pressure. This was explained considering that for MTOW also the highest stiffnesses were obtained. The last two comparisons were made changing strut geometry and wing-strut attachment chordwise position. For the former, it has been observed that the curved model causes an oversizing of the strut, generating a heavier model. In particular, strut axial stiffness is the most increased property. Therefore the associated natural frequencies resulted to be smaller. The differences in tip vertical displacement for trim in cruise are around 20%, while torsional rotation is more or less unchanged for both linear and nonlinear analyses. If the curved strut seems to have a negative effect on flutter analysis, causing the presence of a mode that reaches zero damping (which by the way, as already explained, was not considered flutter), it does not affect very much the linear divergence results. Concerning the wing-strut attachment chordwise position, if the strut is on front spar, a heavier wing and a lighter strut are obtained. On the contrary, if it is on the rear spar, the wing is lighter and the strut is heavier. Moreover, having the strut on the front spar generates the lowest wing tip vertical displacement, which is highest for rear spar attachment. However, this latter condition produced a model that did not pass the verification test. Indeed, the trim in dive presented a twisted downward bending wing (similar problem obtained for ONERA model, but for different reasons), probably due to the presence of a heavy strut and an insufficient attitude for generating enough lift. The inbalance of vertical forces produced the negative behavior. For this reason, gust, flutter and divergence were studied only for front spar attachment. For gust, a different torsional

moment distribution was found with respect to the model with the strut on EA. Again no re-sizing was required. Flutter was not affected by the strut chordwise position, while divergence was increased for front spar strut.

Some studies were conducted to try to understand the characteristics of this unconventional configuration. The main conclusions of this work, along with possible future developments are presented as follows. ONERA strut design has generated some unexpected aeroelastic behavior. Being it very flexible due to its slenderness, aerodynamic loads both due to wing and strut itself produced high deformations that impacted on wing deflection, leading to a downward bending. The problem was adressed by re-designing the component. Indeed, since strut aim is to limit wing root bending moment by limiting wing deflection, some stiffness is required, which results to be a key aspect for sizing. Of course, the increase dimensions, along with the possibility for strut to carry compressive loads, lead to a quite massive component. In order to reduce its weight, composite materials can be employed. In the present work, a very simple laminate has been used, but some particular stacking sequence can be studied such that even higher gains are reached. However, some dedicated aerodynamic analyses must be computed, because the wetted area, as mentioned, is increased, and therefore the friction drag is. Another possibility to keep strut weight limited without excessively incrementing its dimensions, is the introduction of jury memebers, producing a Truss-Braced Wing (TBW) configuration, as the one presented in [21]. Since juries drastically reduce strut effective length, they have an important impact on buckling and, consequently, on sizing. To have a more complete understanding of the aeroelastic behavior of SBW configuration, all the analyses should be extended to nonlinear, because it was evidenced that the results between linear and nonlinear approaches change. In particular, divergence could be interesting in its nonlinear version, because the strut is forward swept. Also nonlinear gust could lead to different conclusions. At the corner point the certification requirements of demonstrating the absence of flutter up to 1.15VD was not satisfied, because of DLM limitations. However, looking at $V - g$s of reference (Section 4.1) and composite curved (Subsection 4.2.3) models, it could happen that flutter is detected inside the flight envelope, because the mode that reached zero damping seems to have an increasing behavior. This means that it could also reach 0.02 damping inside the extended flight envelope. This should not occur for the other composite models. Another aspect concerns the control surfaces. Indeed, in the present work, control surfaces were fixed, because the original model did not account for them. However, especially if flutter would be found inside the flight envelope, a dedicated flutter suppression system could be designed instead of re-optimizing the model introducing flutter constraint (which could lead to weight increase).

Bibliography

[1] IEA, "Aviation analysis," 2022. https://www.iea.org/reports/aviation.

[2] S. Ricci, N. Paletta, S. Defoort, E. Benard, J. E. Cooper, and P. Barabinot, "U-harward: a cs2 eu funded project aiming at the design of ultra high aspect ratio wings aircraft," in *AIAA Scitech 2022 Forum*, p. 0168, 2022.

[3] https://www.u-harward-project.eu/.

[4] L. Cavagna, S. Ricci, and L. Travaglini, "Neocass: an integrated tool for structural sizing, aeroelastic analysis and mdo at conceptual design level," *Progress in Aerospace Sciences*, vol. 47, no. 8, pp. 621–635, 2011.

[5] L. Cavagna, S. Ricci, and L. Riccobene, "Structural sizing, aeroelastic analysis, and optimization in aircraft conceptual design," *Journal of Aircraft*, vol. 48, no. 6, pp. 1840–1855, 2011.

[6] F. Toffol, S. Ricci, *et al.*, "Neopt: an optimization suite for the aeroelastic preliminary design," in *18th International Forum on Aeroelasticity and Structural Dynamics (IFASD 2019)*, pp. 1–19, 2019.

[7] F. Toffol, *Aero-servo-elastic optimization in conceptual and preliminary design*. PhD thesis, Politecnico di Milano, 2021.

[8] https://aircraft.airbus.com/en/aircraft/a320-the-most-successful-aircraft-family-ever/a320neo.

[9] https://www.boeing.com/commercial/737ng/.

[10] P. D. Bravo-Mosquera, F. M. Catalano, and D. W. Zingg, "Unconventional aircraft for civil aviation: A review of concepts and design methodologies," *Progress in Aerospace Sciences*, vol. 131, p. 100813, 2022.

[11] F. Afonso, G. Leal, J. Vale, É. Oliveira, F. Lau, and A. Suleman, "The effect of stiffness and geometric parameters on the nonlinear aeroelastic performance of high

aspect ratio wings," *Proceedings of the Institution of Mechanical Engineers, Part G: Journal of Aerospace Engineering*, vol. 231, no. 10, pp. 1824–1850, 2017.

[12] J. F. Gundlach IV, P.-A. Tetrault, F. H. Gern, A. H. Nagshineh-Pour, A. Ko, J. A. Schetz, W. H. Mason, R. K. Kapania, W. H. Mason, B. Grossman, *et al.*, "Conceptual design studies of a strut-braced wing transonic transport," *Journal of aircraft*, vol. 37, no. 6, pp. 976–983, 2000.

[13] W. Pfenninger, "Design considerations of large subsonic long range transport airplanes with low drag boundary layer suction," *Northrop Aircraft, Inc., Report NAI-54-800 (BLC-67)*, 1954.

[14] W. Pfenninger, "Long-range lfc transport," *NASA, Langley Research Center, Research in Natural Laminar Flow and Laminar-Flow Control, Part 1*, 1987.

[15] H. Park, "The effect on block fuel consumption of a strutted vs. cantilever wing for a short haul transport including strut aeroelastic considerations," *AIAA Paper*, pp. 78–1454, 1978.

[16] R. M. Kulfan and J. D. Vachal, "Wing planform geometry effects on large subsonic military transport airplanes.," tech. rep., BOEING COMMERCIAL AIRPLANE CO SEATTLE WASH, 1978.

[17] P. M. Smith, J. DeYoung, W. A. Lovell, J. E. Price, and G. F. Washburn, "A study of high-altitude manned research aircraft employing strut-braced wings of high-aspect-ratio," tech. rep., 1981.

[18] R. Turriziani, W. Lovell, G. Martin, J. Price, E. Swanson, and G. Washburn, "Preliminary design characteristics of a subsonic business jet concept employing an aspect ratio 25 strut braced wing," tech. rep., 1980.

[19] M. Bhatia, R. K. Kapania, and R. T. Haftka, "Structural and aeroelastic characteristics of truss-braced wings: A parametric study," *Journal of Aircraft*, vol. 49, no. 1, pp. 302–310, 2012.

[20] G. Carrier, O. Atinault, S. Dequand, J. Hantrais-Gervois, C. Liauzun, B. Paluch, A. Rodde, and C. Toussaint, "Investigation of a strut-braced wing configuration for future commercial transport," in *28th Congress of the International Council of the Aeronautical Sciences*, pp. 2012–1, ICAS Bonn, 2012.

[21] C. Droney, N. Harrison, and G. Gatlin, "Subsonic ultra-green aircraft research: transonic truss-braced wing technical maturation," in *Proceedings of the 31st Congress of*

the International Council of the Aeronautical Sciences, Belo Horizon, Brazil, pp. 9–14, 2018.

[22] M. Delavenne, E. Benard, S. Defoort, C. David, N. Fabbiane, J. Schotte, G. Arnoult, and G. Carrier, "Multi-fidelity weight analyses for high aspect ratio strut-braced wings preliminary design," in *IOP Conference Series: Materials Science and Engineering*, vol. 1226, p. 012009, IOP Publishing, 2022.

[23] J. M. Grasmeyer, A. Naghshineh, P. Tetrault, B. Grossman, R. Haftka, R. Kapania, W. Mason, and J. Schetz, "Multidisciplinary design optimization of a strut-braced wing aircraft with tip-mounted engines," *MAD Center Report MAD*, pp. 98–01, 1998.

[24] R. Cavallaro and L. Demasi, "Challenges, ideas, and innovations of joined-wing configurations: a concept from the past, an opportunity for the future," *Progress in Aerospace Sciences*, vol. 87, pp. 1–93, 2016.

[25] F. Gern, J. Gundlach, A. Ko, A. Naghshineh-Pour, E. Sulaeman, P.-A. Tetrault, B. Grossman, R. Kapania, W. Mason, J. Schetz, *et al.*, "Multidisciplinary design optimization of a transonic commercial transport with a strut-braced wing," tech. rep., SAE Technical Paper, 1999.

[26] F. H. Gern, A. H. Naghshineh, E. Sulaeman, R. K. Kapania, and R. T. Haftka, "Flexible wing model for structural sizing and multidisciplinary design optimization of a strut-braced wing," in *41st Structures, Structural Dynamics and Materials Meeting*, no. AIAA Paper 2000-1327, 2000.

[27] O. Gur, M. Bhatia, J. A. Schetz, W. H. Mason, R. K. Kapania, and D. N. Mavris, "Design optimization of a truss-braced-wing transonic transport aircraft," *Journal of aircraft*, vol. 47, no. 6, pp. 1907–1917, 2010.

[28] N. A. Meadows, J. A. Schetz, R. K. Kapania, M. Bhatia, and G. Seber, "Multidisciplinary design optimization of medium-range transonic truss-braced wing transport aircraft," *Journal of Aircraft*, vol. 49, no. 6, pp. 1844–1856, 2012.

[29] W. Mallik, R. K. Kapania, and J. A. Schetz, "Effect of flutter on the multidisciplinary design optimization of truss-braced-wing aircraft," *Journal of Aircraft*, vol. 52, no. 6, pp. 1858–1872, 2015.

[30] I. Chakraborty, T. Nam, J. R. Gross, D. N. Mavris, J. A. Schetz, and R. K. Kapania, "Comparative assessment of strut-braced and truss-braced wing configurations using multidisciplinary design optimization," *Journal of Aircraft*, vol. 52, no. 6, pp. 2009–2020, 2015.

[31] G. G. Carrier, G. Arnoult, N. Fabbiane, J.-S. Schotte, C. David, S. Defoort, E. Benard, and M. Delavenne, "Multidisciplinary analysis and design of strut-braced wing concept for medium range aircraft," in *AIAA SCITECH 2022 Forum*, p. 0726, 2022.

[32] D. W. Zingg, T. Chau, A. L. Gray, and T. A. Reist, "A multifidelity multidisciplinary approach to unconventional aircraft development and assessment with application to the strut-braced wing and hybrid wing-body configurations," in *33rd Congress of the International Council of the Aeronautical Sciences*, 2022.

[33] F. Toffol, N. Fonzi, and S. Ricci, "Non-linear aeroelastic capabilities in neocass suite," in *AIAA SCITECH 2023 Forum*, p. 2406, 2023.

[34] A. Sikora, "European green deal–legal and financial challenges of the climate change," in *Era Forum*, vol. 21, pp. 681–697, Springer, 2021.

List of Figures

List of Tables

List of Symbols

Variable	Description	SI unit
R	range	m
V_{TAS}	true airspeed velocity	$\frac{\mathrm{m}}{\mathrm{s}}$
g	gravity acceleration	$\frac{\mathrm{m}}{\mathrm{s}^2}$
$\frac{L}{D}$	aerodynamic efficiency	-
SFC	specific fuel consumption	$\frac{\mathrm{s}}{\mathrm{m}}$
W_{MTOW}	Maximum Take-Off Weight	kg
W_{fuel}	fuel weight	kg
C_{Di}	coefficient of induced drag	-
C_L	coefficient of lift	-
AR	aspect ratio	-
e	Oswald coefficient	-
t	thickness	m
c	chord	m
M_{cruise}	Mach in cruise	-
M_{dive}	Mach in dive	-
σ	normal stress	MPa
τ	transverse stress	MPa
N	axial force	N
$M_{bending_1}$	out-of-plane bending moment	Nm
$M_{bending_2}$	in-plane bending moment	Nm
M_{torque}	torsional moment	Nm
T_1	out-of-plane shear force	N
T_2	in-plane shear force	N

Variable	Description	SI unit
$\mathbf{E}$	Young modulus	GPa
$\boldsymbol{\nu}$	Poisson's ratio	-
$\mathbf{G}$	Shear Young modulus	GPa
$\boldsymbol{\rho}$	density	$\frac{\text{kg}}{\text{m}^3}$
$\boldsymbol{\sigma_{yield}}$	yielding stress	MPa
$\mathbf{M}$	Mach	-
$\mathbf{h}$	altitude	m
$\mathbf{N}_z$	vertical load factor	g
$\mathbf{V}$	velocity	$\frac{\text{m}}{\text{s}}$
VD	design dive speed	$\frac{\text{m}}{\text{s}}$
VC	design cruise speed	$\frac{\text{m}}{\text{s}}$
VF	flap design speed	$\frac{\text{m}}{\text{s}}$
VA	manoeuvering speed	$\frac{\text{m}}{\text{s}}$
VS	stall clean configuration speed	$\frac{\text{m}}{\text{s}}$
VFLAND	stall landing configuration speed	$\frac{\text{m}}{\text{s}}$
VCLIMB	climb speed	$\frac{\text{m}}{\text{s}}$
$\boldsymbol{K}$	structural stiffness matrix	$\frac{\text{N}}{\text{m}}$
$\boldsymbol{u}$	structural displacement	m
$\boldsymbol{M}$	structural mass matrix	kg
$\boldsymbol{\ddot{u}}$	structural acceleration	$\frac{\text{m}}{\text{s}^2}$
$\boldsymbol{\delta}$	trim parameters	-
q	dynamic pressure	$\frac{\text{kg}}{\text{ms}^2}$
$[\boldsymbol{AICS}]$	generalized aerodynamic loads due to structural displacement	m
$[\boldsymbol{P^a}]$	aerodynamic loads due to trim parameters	-
α	angle of attack	deg
δ_e	equilibrator deflection	deg
s	Laplace variable	$\frac{1}{\text{s}}$
p	nondimensional Laplace variable	-
V_∞	stream speed	$\frac{\text{m}}{\text{s}}$
k	reduced frequency	-

Variable	Description	SI unit
$\boldsymbol{M_{hh}}$	reduced structural mass matrix	kg
$\boldsymbol{C_{hh}}$	reduced structural damping matrix	$\frac{\text{kg}}{\text{s}}$
$\boldsymbol{K_{hh}}$	reduced structural stiffness matrix	$\frac{\text{N}}{\text{m}}$
$\boldsymbol{Q_{hh}}$	reduced generalized aerodynamic loads due to structural displacement	m
$\boldsymbol{q}$	generalized structural displacement	m
g	damping factor	-
f	frequency	Hz
$\boldsymbol{Q_{hg}}$	reduced generalized aerodynamic loads due to gust	ms
V_G	gust velocity	$\frac{\text{m}}{\text{s}}$
$\boldsymbol{K_g}$	geometrical stiffness matrix	$\frac{\text{N}}{\text{m}}$
$\boldsymbol{K_m}$	material stiffness matrix	$\frac{\text{N}}{\text{m}}$
$\boldsymbol{K_T}$	tangent stiffness matrix	$\frac{\text{N}}{\text{m}}$
$\boldsymbol{f_{int}}$	internal forces	N
q_{max}	maximum reachable dynamic pressure	$\frac{\text{kg}}{\text{ms}^2}$
q_{div}	divergence dynamic pressure	$\frac{\text{kg}}{\text{ms}^2}$

Ringraziamenti

Durante il primo semestre del primo anno, tra i corsi da seguire c'era disegno tecnico. Un pomeriggio a settimana avevamo questo laboratorio dove dovevamo disegnare le viste di componenti meccanici, e alla fine delle ore dovevamo portare le tavole con i disegni al prof e agli assistenti affinché ci convalidassero la partecipazione. Ero al poli da circa un mese, e un pomeriggio non ero riuscita a finire tutte le viste che ci avevano assegnato, per cui quando ero andata in cattedra per la firma ero un po' agitata. Il prof era impegnato, quindi mi sono rivolta all'assistente e gli ho detto che non avevo fatto in tempo a finire tutto. Lui mi ha detto testualmente "l'importante è arrivare". Forse è stato profetico per il resto di tutto il mio percorso universitario.
Essendo i miei studi volti al termine (forse), è arrivata la parte divertente: i ringraziamenti. I primi vanno al mio relatore, il professor Sergio Ricci, il quale mi ha permesso di capire come lavora un bravo ingegnere, mi ha ascoltata anche quando non ero soddisfatta del mio lavoro e mi ha coinvolta partecipando attivamente a riunioni di progetto dando un senso più concreto ai miei studi. Non so se sono stata particolarmente fortunata io o se sono stati sfortunati i miei compagni con i loro relatori, in ogni caso grazie. Successivamente ringrazio Luca Marchetti e Nicola Fonzi, che mi hanno seguito nelle prime fasi della tesi. A parte ringrazio Francesco Toffol, che mi ha aiutata infinitamente. Senza di lui probabilmente avrei fatto un decimo di ciò che ho realmente fatto. Grazie per essere stato così paziente.
Grazie a tutte le persone che ho conosciuto in questi anni, con cui ho legato, con cui ho bevuto alla rossa, con cui mi sono sfogata: Ste, Simo, Niil, Luca, Salvo per citarne alcuni. Grazie ai miei compagni di corso, andando con ordine cronologico, le ragazze: Chiara, Erika, Serena, Silvia. Alla faccia di chi diceva, quando abbiamo iniziato, che a ingegneria ci sono solo ragazzi. Non vedo l'ora di rivedervi tutte insieme. E grazie a Diego, che mi ha accompagnato negli anni di magistrale. Ex, uai, zed. Grazie a chi c'è stato e poi si è perso. Ma soprattutto grazie a Sabrina. Non avrei mai pensato di uscire dal poli con una amicizia così sincera e genuina. Tu mi hai fatto il regalo più grande: mi hai fatto divertire. Sei stata una compagna di studi perfetta, con cui ho potuto condividere ogni, letteralmente ogni, pensiero. Adesso andiamo in B12 e ci rubiamo il nostro tavolino e

guai a chi ci dice qualcosa. Grazie amica mia.
Infine grazie alla mia famiglia per avermi sostenuto economicamente durante tutti questi anni. Grazie a mio papà Marco, se ho scelto ingegneria evidentemente qualcosa mi hai insegnato. Grazie a mia mamma Sonia, la mia fan numero uno, la persona che mi ha sempre fatto credere in me stessa, mi vien da ridere se penso che mi facevi i complimenti anche solo quando mi iscrivevo agli esami. Sei stata fondamentale per la mia autostima. (E ovviamente sei la mamma migliore del mondo). Grazie a mia sorella Francesca, che è sì mia sorella, ma soprattutto mia amica, per avermi accompagnato durante tutti gli studi della mia vita, per avermi facilitato la strada chissà quante volte, per i confronti costruttivi, per la tua infinita intelligenza, per essere così stimolante. Per finire, grazie ad Anna, la mia migliore amica, che nonostante la distanza c'è sempre stata. Una volta mi hai chiesto come fosse possibile che una come me fosse amica di una come te, io mi chiedo il contrario. Sei speciale. E grazie a Lorenzo, che è stato al mio fianco per tutti questi lunghi anni, che si è subito le mie ansie, le mie assenze, e ha sempre pazientato e mi ha sempre capita. Grazie amore mio, ora possiamo andare ad Andalo.

Acknowledgements

This thesis has been partially supported by CS2-U-HARWARD Project.
The U-HARWARD Project has received funding from Clean Sky 2 Joint Undertaking (JU) under grant agreement number 886552. The JU receives support from the European Union's Horizon 2020 research and innovation program and the Clean Sky 2 JU members other than the Union.